PERGAMON

Deep-Sea Research I 47 (2000) 1899–1936

DEEP-SEA RESEARCH
PART I

Evidence for strong sediment redistribution by bottom currents along the southeast Indian ridge

L. Dezileau[a,*], G. Bareille[b,1], J.L. Reyss[a], F. Lemoine[a]

[a]*Laboratoire des Sciences du Climat et de l'Environnement, Laboratoire mixte C.E.A.-C.N.R.S., Gif sur Yvette, 91198 Gif sur Yvette cedex, France*

[b]*Département de Géologie et d'Océanographie, Université de Bordeaux I, U.A. 197, 33405 Talence cedex, France*

Abstract

Understanding whether vigorous bottom currents redistribute biogenic components coming from the surface water is critical to evaluating the results from paleoenvironmental reconstructions based on sediment accumulation rates in the Southern Ocean. A large contourite drift along the southern flank of the Southeast Indian Ridge (SEIR) is recognized in published sediment thickness maps. We use the ^{230}Th method to estimate the contribution of advected sediments to the bulk sediment and rare-earth elements (REE) and trace-element compositions to determine the possible differences in sedimentary origin of the transported material. Magnetic susceptibility and "focusing factor" distributions suggest that (a) accumulation and sediment redistribution on the contourite drift have occurred throughout the last 40 ka, (b) the lateral transport of biogenous and detrital material represents 50–90% of the input at the foot of the SEIR, and (c) transport was even higher during glacial periods. Both REE profiles and trace-element ratios (La_n/Tb_n and Th/Sc) reveal that during the last glacial period, the terrigenous particles were mainly of volcanogenic origin, i.e., from the Crozet and Kerguelen slopes. The more significant contribution from the volcanic sources during the last glacial maximum is consistent with the action of the Antarctic Circumpolar Current-Circumpolar Deep Water (ACC-CDW). In addition, the formation of this tongue would be strongly linked to the long-term interactions between the Antarctic Bottom Water (AABW) and the ACC-CDW.

* Corresponding author. Fax: 0033-1-69-82-35-68.

E-mail address: laurent.dezileau@lsce.cnrs-gif.fr (L. Dezileau).

[1] Present address: LCABIE, CNRS EP 132, Université de Pau et des pays de l'Adour, Helioparc, 2 Av. Président Angot, 64 000 PAU, France.

0967-0637/00/$ - see front matter
PII: S0967-0637(00)00008-X

1. Introduction

One of the most exciting discoveries of this decade regarding the global carbon cycle was the demonstration that the carbon dioxide content of the glacial age atmosphere was about one-third lower than typical Holocene values (190 versus 280 ppm). The evidence is contained in the air trapped within polar ice (Barnola et al., 1987). The Southern Ocean seems to be a key area to explain the glacial lowering of atmospheric CO_2. Investigators have attempted to link variations in CO_2 content, recorded in ice cores, to the variability of the Southern Ocean productivity (Knox and McElroy, 1984; Sarmiento and Toggweiler, 1984; Martin, 1990).

Several tools, such as stable isotopes, trace element and particle-reactive element ratios, redox-sensitive trace element concentrations, and accumulation rates of biogenic detritus buried on the seafloor, have been used to infer past Southern Ocean productivity (Labeyrie and Duplessy, 1985; Boyle, 1988; Keigwin and Boyle, 1989; Charles and Fairbanks, 1990; Mortlock et al., 1991; Charles et al., 1991; Kumar et al., 1995; Francois et al., 1997; Anderson et al., 1998; Bareille et al., 1998). However, estimates of past changes in Southern Ocean productivity are still uncertain. Indeed, although there is a large choice in the paleoproductivity tools, they lead to ambiguous interpretations originating in the significant uncertainties related to the precise meaning of each tool, and to various processes altering the link between the surface productivity and the sedimentary record. For example, sediment redistribution by deep currents is a particularly significant process, because it can significantly dilute the vertical rain rate of biogenic particles. It also contributes to the preservation state of biogenic components and influences steady-state redox conditions in the sediment by advecting metabolizable organic matter.

In the Southern Ocean, sediment redistribution may be especially significant because of the relatively strong currents associated with the Antarctic Circumpolar Current and the Antarctic Bottom Water. Evidence for strong currents is found in scour zones and in contourite deposits, such as along the eastern margin of the Kerguelen Plateau (Kennett and Watkins, 1975; Kennett and Watkins, 1976; Kolla and Biscaye, 1976; Houtz et al., 1977; Kolla et al., 1978). There is also evidence for current-driven sediment redistribution from studies on the distribution of particulate matter in the water column. Within the Crozet Basin and around the north end of the Kerguelen Plateau, strong bottom-water activity is suggested by strong excess turbidity values (Kolla and Biscaye, 1976; McCave, 1986).

From a simple model that compares the expected and measured accumulation rates of ^{230}Th in the sediment, Suman and Bacon (1989) argue that the lateral sediment redistribution could be quantified and the vertical rain rates could be reconstructed even from cores collected in areas where sediment deposition is dominated by lateral transport by bottom currents. Such an approach using ^{230}Th has been recently used in some sedimentary cores from the Southern Ocean (Kumar et al., 1995; Frank et al., 1996; Francois et al., 1997; Anderson et al., 1998). The laterally advected contribution of sediment has been shown to exceed the vertical particle flux by an order of magnitude in some localities in the Indian sector (Francois et al., 1997) and the Atlantic sector (Kumar et al., 1995; Frank et al., 1996; Anderson et al., 1998) of the

Southern Ocean. However, this method has not been used to understand the lateral sediment input at the scale of the ocean basin. Consequently, little information is available about the spatially current-controlled sediment redistribution, how redistribution varies during glacial–interglacial periods and what implications sediment redistribution may have for paleoclimatic and paleoproductivity reconstructions.

In this study we investigated the effects of water-mass circulation on deep marine sedimentation along the southern flank of the Southeast Indian Ridge (SEIR). In particular, by combining the sediment thickness map from Houtz et al. (1977) with physical (magnetic susceptibility) and sedimentological (detrital and opal contents) measurements, we qualitatively demonstrate that long-term current-controlled sedimentation along the SEIR occurred also at the scale of the last glacial–interglacial cycle (40 ka). With the ^{230}Th method and "focusing factor" maps, we quantitatively estimate spatial and temporal (glacial–interglacial) accumulation variability of laterally advected sediment on the SEIR for the last 40 ka. Finally, trace-element compositions can be used to indicate possible differences in sedimentary origin, providing insight into the possible mechanisms of sedimentary input.

2. Oceanography

At present, water-mass circulation in the Southern Ocean is controlled by: (1) wind stress, which drives the eastward-flowing Antarctic Circumpolar Current (ACC); (2) deep convection, which renews bottom and deep waters; and (3) cyclonic subpolar gyres (Weddell, Ross and East Indian) (Nowlin, 1991). The ACC constitutes the largest current system in the World Ocean, transporting about $100–140 \times 10^6$ m^3 s^{-1} (Sv) of water in an eastward direction (Orsi et al., 1995). In the Indian sector, the ACC is strongly concentrated in a single narrow band (Fig. 1), formed by the confluence of the Subantarctic Front (SAF) and the Subtropical Front (STF) to the north of the Crozet and Kerguelen Plateaus (Park et al., 1991, 1993). This narrow frontal zone, with a width of 2–3° latitude, hugs the northern flank of the Kerguelen Plateau and contains about 80% of the ACC transport to the southeastern Indian sector. This main flow path of about 100 Sv, lying between 46°S and 43°S, is controlled by the topography of the Kerguelen Plateau and generates high energy on the northern part of this plateau (Park and Saint-Guily, 1992).

In the South Indian Basin (SIB), the movement of Antarctic Bottom Water (AABW), which originates along the Adélie Land coast and in the Ross Sea (Jacobs et al., 1970; Eittreim et al., 1972a, b; Rintoul, 1998), is clockwise. AABW, which travels westward and close to the Antarctic continent, is diverted to the north by the Kerguelen Plateau (Fig. 1), until it flows east along the southern margin of the SEIR (Kennett and Watkins, 1975, 1976; Kolla et al., 1976b). The influence of the northward-moving AABW on sediment transport and seafloor was previously demonstrated to be widespread in the western and northwestern part of the SIB, i.e., along the eastern margin of the Kerguelen Plateau and on the southern margin of the SEIR (Kolla et al., 1976a, 1978). These influences have been inferred from both turbidity, current indications, and bottom photographs (Eittreim et al., 1972a; Kolla et al.,

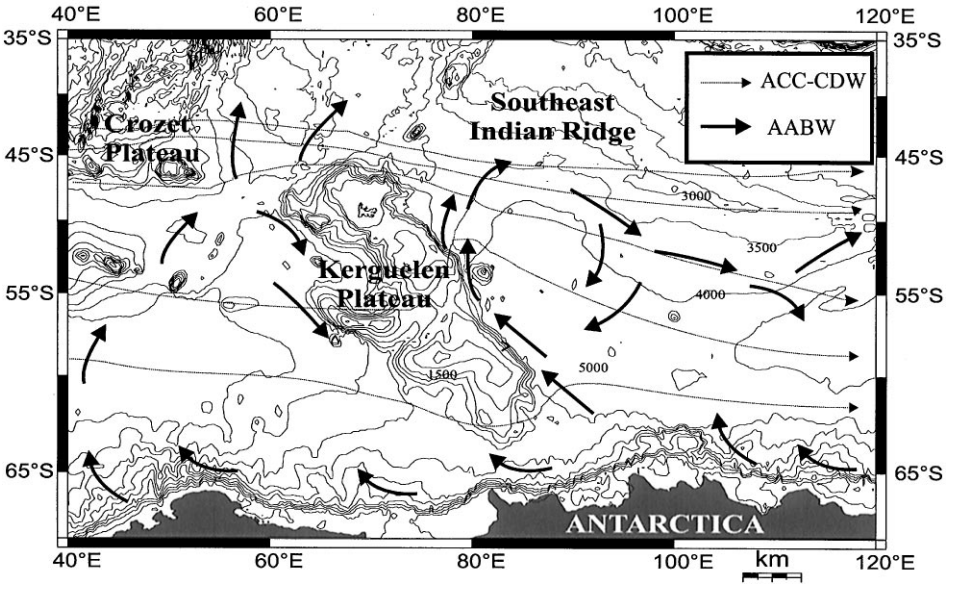

Fig. 1. Circulation patterns of Antarctic Bottom Water (AABW) and the Antarctic Circumpolar Current (ACC) (taken from Kolla et al., 1976; Park and Gambéroni, 1995).

1976a, 1978) and have been attributed to vigorous bottom-water activity. Such strong bottom-water currents have a significant erosive capacity that generates a large nepheloid layer. This layer consists of both terrigenous and biogenous particles from bottom sediments (Barron et al., 1991; Ehrmann and Grobe, 1991). In some places, such as along the western margin of the basin, the AABW particle load mostly settles, building a large sedimentary ridge parallel to the eastern flank of the Kerguelen Plateau (Eittreim et al., 1972a; Houtz et al., 1977). Strong AABW eastward current flow seems to occur at depths of around 4000 m in the northern sector of the SIB, as inferred from sea beds of Mn pavement to abundant nodules (Kennett and Watkins, 1975, 1976). This strong eastward flow of AABW may be enhanced by the addition of high-velocity ACC that is concentrated along the northern flank of the Kerguelen Plateau.

3. Materials, methods and stratigraphic framework

3.1. Core material

Four gravity cores from the southern flank of the SEIR (Table 1, Fig. 2) were analysed for ^{230}Th to quantify the amount of material transported and deposited by bottom currents on the ridge. All cores were collected at water depths between 3000 and 3500 m beneath the eastward-flowing ACC and AABW. We also examined one

Table 1
Locations of the gravity cores studied for $^{230}Th_{ex}^{\circ}$ are in bold. The others were used only for mapping opal and detrital accumulation rates for the Holocene period, or to examine sediment thickness variablity for the last 160 ka

Cores	Longitude (°E)	Latitude (°S)	Water depth (m)
MD 94-102	**79.8**	**43.5**	**3205**
MD 88-768	82.9	45.8	3330
MD 94-103	86.5	45.6	3559
MD 88-767	79.5	46.7	2920
MD 94-108	90.0	46.0	3409
MD 94-109	90.1	44.7	3315
MD 94-104	**88.1**	**46.5**	**3460**
MD 88-769	**90.1**	**46.1**	**3420**
MD 88-770	**96.5**	**46.0**	**3290**
MD 94-107	90.2	47.8	3525
MD 88-771	100.1	49.9	3310
MD 88-772	104.9	50.0	3240
MD 84-527	**51.2**	**43.5**	**3269**
MD 88-773	**109.5**	**52.55**	**2460**
MD 94-106	89.3	48.5	3709
MD 84-552	**73.8**	**54.9**	**1780**

core from the Kerguelen plateau (MD 84-552). All cores were recovered during the APSARA II (1984) and IV (1988) and PACIMA (1994) cruises. We selected cores to cover the frontal zones that constrain the ACC, i.e. from the Subtropical Front to the Polar Front.

Other cores (Table 1), which were the subjects of previous geochemical and magnetic susceptibility studies (Bareille, 1991; Bareille et al., 1994), were also used. These cores were used first to map both detrital and opal accumulation rates for the Holocene and second to investigate spatial and temporal changes in sediment thickness on the SEIR.

The gravity cores were sampled with a resolution of 5–25 cm between samples depending on macroscopical changes in lithology and previously determined stratigraphies. The age resolution ranged from about 200 yr to about 15 000 yr between samples. Cores, were from shallow ridges and were selected from depths near or above the lysocline in order to minimize the effect of dissolution as a variable controlling the carbonate content of the sediment.

3.2. Analytical methods

3.2.1. U and Th isotopes

Uranium and thorium concentrations were measured by α-spectrometry following separation on anion exchange column and deposition onto aluminium foil. Uranium and thorium were analysed following the procedure described by Legeleux (1994). The analytical uncertainty for ^{230}Th concentration due to counting statistics was 5%.

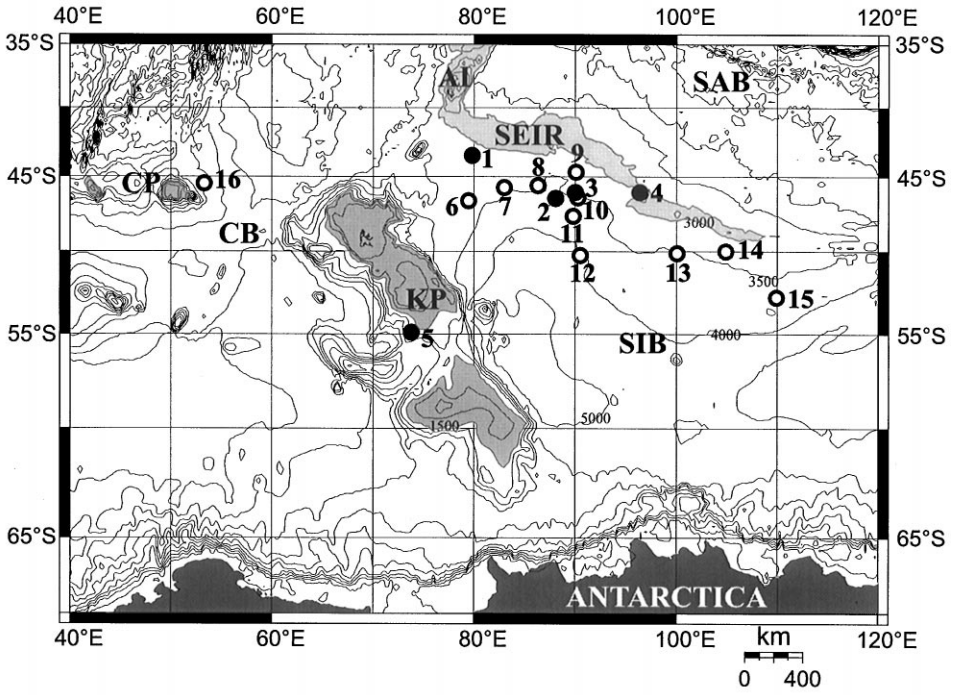

● Cores studied for $^{230}Th_{ex}$

○ Cores with magnetic susceptibility profiles and/or biogenic silica and detrital accumulation rates

1: MD 94-102; **2**: MD 94-104; **3**: MD 88-769; **4**: MD 88-770; **5**: MD 84-552; **6**: MD 88-767;**7**: MD 88-768; **8**: MD 94-103; **9**: MD 94-109; **10**: MD 94-108; **11**: MD 94-107; **12**: MD 94-106; **13**: MD 88-771; **14**: MD 88-772; **15**: MD 88-773; **16**: MD 84-527; Core MD 84-527 and MD 88-773 have been previously studied for $^{230}Th_{ex}$ by François et al. (1992, 1998)

Fig. 2. Topography of the studied area and cores location. CP: Crozet Plateau; CB: Crozet Basin; KP: Kerguelen Plateau; SEIR: Southeast Indian Ridge; SIB: South Indian Basin; SAB: South Australian Basin; AI: Amsterdam Island.

Samples were only occasionally run in duplicate, and uncertainties were less than or equal to those due to counting statistics. Analytical uncertainty in ^{238}U due to counting statistics was 6%. Precisions (1σ) are reported in Table 2.

3.2.2. Rare-earth elements (REE)

Analyses of Th, Sc, La and Tb (Table 3) were carried out by Epithermal Neutron Activation Analysis (ENAA) at the Pierre Süe Laboratory (Saclay, France). Two USGS standards, Mag 1 and A1, were used. Sediment samples and standards were

Table 2
The ^{230}Th, ^{232}Th, ^{238}U and $^{230}Th^{\circ}_{ex}$ activities

Core	Depth (cm)	Age (ka)	^{230}Th (dpm g^{-1})	^{232}Th (dpm g^{-1})	^{238}U (dpm g^{-1})	$^{230}Th^{\circ}_{ex}$ (dpm g^{-1})
MD 94-102	0	6.5	7.65 ± 0.37	0.75 ± 0.05	0.43 ± 0.04	7.66 ± 0.39
	10	8.2	7.29 ± 0.48	0.81 ± 0.06	0.46 ± 0.03	7.35 ± 0.51
	20	9.9	7.12 ± 0.17	0.47 ± 0.02	0.27 ± 0.02	7.50 ± 0.19
	30	11.6	6.69 ± 0.51	0.47 ± 0.05	0.32 ± 0.02	7.14 ± 0.57
	40	13.3	6.44 ± 0.26	0.47 ± 0.03	0.31 ± 0.02	6.97 ± 0.29
	50	15.0	5.01 ± 0.37	0.37 ± 0.04	0.31 ± 0.02	6.64 ± 0.43
	60	16.6	5.65 ± 0.28	0.50 ± 0.04	0.31 ± 0.02	6.25 ± 0.32
	70	17.6	6.33 ± 0.39	0.66 ± 0.06	0.38 ± 0.06	7.00 ± 0.46
	80	20.7	6.64 ± 0.39	0.71 ± 0.05	0.41 ± 0.02	7.54 ± 0.47
	90	24.9	6.58 ± 0.36	0.69 ± 0.05	0.40 ± 0.03	7.78 ± 0.46
	100	29.1	6.64 ± 0.40	0.72 ± 0.05	0.36 ± 0.02	8.16 ± 0.53
	110	32.6	6.30 ± 0.29	0.67 ± 0.04	0.39 ± 0.02	7.98 ± 0.40
	120	34.8	6.23 ± 0.30	0.69 ± 0.04	0.36 ± 0.03	8.05 ± 0.42
	130	35.8	5.25 ± 0.26	0.58 ± 0.04	0.38 ± 0.03	7.65 ± 0.37
	140	36.8	5.05 ± 0.20	0.44 ± 0.03	0.33 ± 0.03	6.71 ± 0.29
	150	40.3	5.45 ± 0.35	0.57 ± 0.05	0.32 ± 0.01	7.45 ± 0.50
	160	43.7	4.75 ± 0.21	0.44 ± 0.03	0.25 ± 0.01	6.74 ± 0.32
MD 94-104	50	4.3	9.90 ± 0.31	0.35 ± 0.02	0.29 ± 0.03	10.05 ± 0.32
	100	8.6	8.90 ± 0.50	0.43 ± 0.04	0.24 ± 0.03	9.36 ± 0.54
	130	11.1	7.38 ± 0.36	0.43 ± 0.04	0.31 ± 0.03	7.89 ± 0.39
	160	13.0	8.93 ± 0.32	0.61 ± 0.03	0.55 ± 0.02	9.63 ± 0.36
	180	13.8	8.41 ± 0.26	0.84 ± 0.04	1.01 ± 0.05	8.92 ± 0.30
	200	14.6	9.38 ± 0.38	1.15 ± 0.07	3.48 ± 0.14	9.53 ± 0.44
	230	16.0	8.94 ± 0.40	1.30 ± 0.09	3.40 ± 0.47	9.03 ± 0.47
	300	19.1	7.51 ± 0.30	1.07 ± 0.07	3.34 ± 0.16	7.61 ± 0.36
	380	22.7	8.52 ± 0.32	1.32 ± 0.07	3.21 ± 0.10	8.98 ± 0.39
	470	27.5	8.16 ± 0.42	1.45 ± 0.09	2.19 ± 0.09	8.99 ± 0.54
	600	35.1	6.94 ± 0.40	0.94 ± 0.07	1.98 ± 0.16	8.25 ± 0.56
	640	37.4	5.48 ± 0.26	0.68 ± 0.06	1.98 ± 0.09	6.54 ± 0.37
	700	41.0	7.45 ± 0.46	1.15 ± 0.08	1.73 ± 0.19	9.35 ± 0.68
	800	47.0	7.63 ± 0.46	0.97 ± 0.08	2.34 ± 0.12	9.84 ± 0.70
MD 88-769	15	8.5	7.98 ± 0.78	0.31 ± 0.06	0.17 ± 0.02	8.44 ± 0.85
	20	9.7	7.13 ± 0.50	0.31 ± 0.04	0.18 ± 0.02	7.59 ± 0.55
	25	11.0	6.66 ± 0.35	0.26 ± 0.03	0.18 ± 0.02	7.21 ± 0.39
	35	13.4	7.25 ± 0.35	0.40 ± 0.03	0.24 ± 0.03	7.94 ± 0.40
	52	15.7	7.80 ± 0.47	0.80 ± 0.06	0.29 ± 0.03	8.52 ± 0.55
	64	16.4	10.21 ± 0.69	1.06 ± 0.09	0.88 ± 0.04	11.15 ± 0.80
	76	17.2	9.94 ± 0.72	1.12 ± 0.10	2.65 ± 0.18	10.50 ± 0.84
	85	18.0	9.55 ± 0.90	1.19 ± 0.14	4.40 ± 0.26	9.72 ± 1.06
	95	19.5	10.14 ± 0.55	1.01 ± 0.07	5.07 ± 0.30	10.47 ± 0.66
	109	21.5	11.51 ± 0.73	1.24 ± 0.09	5.11 ± 0.59	12.13 ± 0.89
	130	24.2	11.53 ± 0.45	1.40 ± 0.07	4.58 ± 0.18	12.42 ± 0.56
	149	26.5	8.91 ± 0.85	1.11 ± 0.13	4.27 ± 0.24	9.40 ± 1.08

(*continued on next page*)

Table 2 (*continued*)

Core	Depth (cm)	Age (ka)	^{230}Th (dpm g^{-1})	^{232}Th (dpm g^{-1})	^{238}U (dpm g^{-1})	$^{230}Th^{\circ}_{ex}$ (dpm g^{-1})
	170	29.1	9.72 ± 0.66	1.26 ± 0.10	3.45 ± 0.19	10.50 ± 0.86
	190	31.7	9.82 ± 0.46	1.86 ± 0.06	3.12 ± 0.16	10.11 ± 0.61
	210	34.3	8.17 ± 0.40	0.73 ± 0.05	2.60 ± 0.22	9.75 ± 0.56
	230	36.8	7.15 ± 0.48	0.65 ± 0.08	2.42 ± 0.16	8.62 ± 0.67
	250	39.6	9.39 ± 0.48	0.87 ± 0.06	3.01 ± 0.17	11.53 ± 0.68
	270	42.5	8.10 ± 0.86	0.92 ± 0.12	2.05 ± 0.14	10.41 ± 0.26
MD 88-770	19	7.3	6.06 ± 0.28	0.11 ± 0.02	0.13 ± 0.02	6.41 ± 0.28
	39	10.2	4.69 ± 0.16	0.12 ± 0.01	0.16 ± 0.01	5.07 ± 0.17
	49	11.7	5.57 ± 0.19	0.17 ± 0.01	0.14 ± 0.01	6.09 ± 0.22
	97	16.6	9.81 ± 0.46	0.54 ± 0.04	5.93 ± 0.33	10.07 ± 0.54
	117	18.2	9.06 ± 0.77	0.64 ± 0.08	6.13 ± 0.32	9.13 ± 0.90
	159	19.8	9.41 ± 0.46	0.69 ± 0.05	5.50 ± 0.21	9.75 ± 0.55
	198	21.2	8.20 ± 0.53	0.60 ± 0.08	4.38 ± 0.24	8.55 ± 0.64
	278	24.6	8.53 ± 0.27	0.59 ± 0.03	4.33 ± 0.33	9.10 ± 0.34
	339	28.1	6.74 ± 0.33	0.52 ± 0.04	4.45 ± 0.23	7.01 ± 0.43
	419	34.0	4.94 ± 0.48	0.19 ± 0.05	3.76 ± 0.24	5.08 ± 0.63
	519	43.2	6.44 ± 0.31	0.40 ± 0.03	3.59 ± 0.22	7.39 ± 0.46
MD 54-552	19	7.7	2.18 ± 0.08	0.08 ± 0.01	0.18 ± 0.02	2.28 ± 0.08
	29	8.0	2.04 ± 0.11	0.06 ± 0.02	0.18 ± 0.03	2.14 ± 0.12
	39	8.3	1.81 ± 0.07	0.07 ± 0.02	0.19 ± 0.02	1.90 ± 0.08
	49	8.5	1.62 ± 0.09	0.09 ± 0.03	0.19 ± 0.03	1.68 ± 0.10
	59	8.7	1.74 ± 0.11	0.07 ± 0.02	0.19 ± 0.03	1.83 ± 0.12
	69	9.3	1.85 ± 0.13	0.12 ± 0.03	0.21 ± 0.02	1.92 ± 0.14
	77	9.7	1.41 ± 0.09	0.07 ± 0.03	0.23 ± 0.02	1.48 ± 0.10
	89	10.3	1.81 ± 0.08	0.10 ± 0.02	0.18 ± 0.01	1.92 ± 0.09
	97	10.7	1.95 ± 0.16	0.24 ± 0.04	0.30 ± 0.03	2.00 ± 0.17
	109	11.6	2.40 ± 0.06	0.26 ± 0.01	0.37 ± 0.02	2.47 ± 0.06
	118	12.0	2.29 ± 0.18	0.24 ± 0.04	0.31 ± 0.05	2.38 ± 0.20
	127	12.3	2.72 ± 0.21	0.43 ± 0.06	0.48 ± 0.03	2.74 ± 0.24
	139	12.7	3.64 ± 0.26	0.74 ± 0.08	0.72 ± 0.11	3.57 ± 0.30
	149	13.1	3.77 ± 0.25	0.82 ± 0.07	0.67 ± 0.08	3.69 ± 0.29
	157	13.9	4.34 ± 0.20	1.01 ± 0.07	0.80 ± 0.05	4.24 ± 0.23
	169	18.1	4.18 ± 0.31	1.06 ± 0.09	0.79 ± 0.06	4.18 ± 0.37
	179	20.1	4.46 ± 0.29	1.01 ± 0.09	1.15 ± 0.14	4.38 ± 0.36
	199	23.9	4.28 ± 0.13	1.02 ± 0.04	1.16 ± 0.03	4.45 ± 0.16
	219	33.0	4.20 ± 0.22	0.94 ± 0.06	0.68 ± 0.03	4.90 ± 0.30
	239	41.0	3.72 ± 0.23	0.79 ± 0.05	0.57 ± 0.02	4.71 ± 0.34

enclosed in aluminium bags; thus corrections were required and were made for each element by subtracting the contribution of the element from the bag (this correction is $< 5\%$). After irradiation, sediment samples and standards were measured with an HP Ge detector (FWMH 1.7 keV at 1332 keV; relative efficiency: 20%) at the Laboratoire des Sciences du Climat et de l' Environnement.

Table 3
La_n/Tb_n and Th/Sc ratio

Core	Depth (cm)	Age (ka)	La (ppm)	Tb (ppm)	La_n/Tb_n	Fe (%)	Th (ppm)	Sc (ppm)	Th/Sc
MD 94-102	20	9.9	12.03 ± 0.60	0.30 ± 0.02	1.20 ± 0.09	0.79 ± 0.02	1.76 ± 0.09	2.77 ± 0.14	0.64 ± 0.04
Gravity Core	30	11.6	11.84 ± 0.59	0.32 ± 0.02	1.11 ± 0.08	0.91 ± 0.02	1.82 ± 0.09	3.18 ± 0.16	0.57 ± 0.04
	50	15.0	11.09 ± 0.55	0.39 ± 0.02	0.85 ± 0.06	1.62 ± 0.03	1.82 ± 0.09	5.79 ± 0.29	0.32 ± 0.02
	70	17.6	12.95 ± 0.65	0.50 ± 0.03	0.76 ± 0.05	2.56 ± 0.05	2.57 ± 0.13	9.13 ± 0.46	0.28 ± 0.02
	80	20.7	14.92 ± 0.75	0.52 ± 0.03	0.86 ± 0.06	2.96 ± 0.06	2.90 ± 0.14	10.59 ± 0.53	0.27 ± 0.02
	90	24.9	16.05 ± 0.80	0.55 ± 0.03	0.85 ± 0.06	2.85 ± 0.06	2.97 ± 0.15	10.72 ± 0.54	0.28 ± 0.02
	100	29.1	18.18 ± 0.91	0.59 ± 0.03	0.92 ± 0.07	3.05 ± 0.06	3.17 ± 0.16	11.05 ± 0.55	0.29 ± 0.02
	120	34.8	13.59 ± 0.69	0.46 ± 0.02	0.91 ± 0.06	2.03 ± 0.04	2.35 ± 0.12	7.19 ± 0.36	0.33 ± 0.02
	140	36.8	11.88 ± 0.59	0.40 ± 0.02	0.89 ± 0.06	1.52 ± 0.04	2.17 ± 0.11	6.41 ± 0.32	0.34 ± 0.02
	150	40.3	11.60 ± 0.58	0.38 ± 0.02	0.92 ± 0.06	1.62 ± 0.03	2.16 ± 0.11	6.00 ± 0.30	0.36 ± 0.03
MD 94-104	50	4.3	9.60 ± 0.48	0.27 ± 0.02	1.07 ± 0.10	1.01 ± 0.02	1.96 ± 0.10	3.80 ± 0.19	0.52 ± 0.04
Gravity Core	100	8.6	7.70 ± 0.39	0.24 ± 0.02	0.97 ± 0.09	2.36 ± 0.05	4.03 ± 0.20	8.27 ± 0.41	0.49 ± 0.03
	180	13.8	13.50 ± 0.68	0.47 ± 0.04	0.86 ± 0.08	4.61 ± 0.09	6.03 ± 0.30	14.20 ± 0.71	0.42 ± 0.03
	200	14.6	20.46 ± 1.02	0.69 ± 0.03	0.89 ± 0.05	3.79 ± 0.08	5.01 ± 0.25	11.30 ± 0.57	0.44 ± 0.03
	300	19.1	20.63 ± 1.03	0.74 ± 0.04	0.84 ± 0.06	4.34 ± 0.09	4.57 ± 0.24	13.78 ± 0.69	0.35 ± 0.02
	380	22.7	21.62 ± 1.09	0.56 ± 0.03	0.99 ± 0.07	4.42 ± 0.09	5.21 ± 0.26	14.12 ± 0.71	0.37 ± 0.03
	600	35.1	14.53 ± 0.73	0.42 ± 0.02	1.04 ± 0.07	3.04 ± 0.06	3.64 ± 0.18	8.45 ± 0.42	0.43 ± 0.03
	640	37.4	11.41 ± 0.57	0.36 ± 0.02	0.98 ± 0.07	2.23 ± 0.04	2.51 ± 0.13	6.58 ± 0.33	0.38 ± 0.03
KR 85 03	10	3.4	8.00 ± 0.40	0.19 ± 0.02	1.26 ± 0.14	2.57 ± 0.05	5.58 ± 0.28	11.58 ± 0.58	0.48 ± 0.03
Box Core	38	8.8	10.80 ± 0.54	0.28 ± 0.03	1.15 ± 0.13	3.30 ± 0.07	6.18 ± 0.31	12.20 ± 0.61	0.51 ± 0.04
MD 88-769	35	13.4	9.26 ± 0.46	0.29 ± 0.01	0.96 ± 0.07	1.06 ± 0.02	1.82 ± 0.09	4.00 ± 0.20	0.46 ± 0.03
Gravity Core	95	19.5	18.70 ± 0.94	0.64 ± 0.03	0.88 ± 0.06	3.51 ± 0.07	4.36 ± 0.22	13.50 ± 0.68	0.32 ± 0.02
	130	24.2	19.40 ± 0.97	0.65 ± 0.03	0.90 ± 0.06	4.02 ± 0.08	5.19 ± 0.26	15.10 ± 0.76	0.34 ± 0.02
	149	26.5	19.64 ± 0.98	0.54 ± 0.03	0.92 ± 0.07	3.56 ± 0.07	5.22 ± 0.26	13.76 ± 0.69	0.38 ± 0.03
	230	36.8	10.6 ± 0.5	0.32 ± 0.02	0.99 ± 0.07	1.80 ± 0.04	2.26 ± 0.11	6.15 ± 0.31	0.37 ± 0.03

(*continued on next page*)

Table 3 (*continued*)

Samples	Sources	Type	La_n/Tb_n
	Potential volcanic detrital sources		
S-E Indian ridge	Dosso et al. (1988)	Basalt	0.13
St-Paul Island	Dosso et al. (1988)	Basalt	0.50
Kerguelen Island 145	Weis et al. (1998)	Basalt	0.85
Kerguelen Island 83	Weis et al. (1998)	Basalt	0.65
Kerguelen Island 747	Salters et al. (1992)	Basalt	0.44
Kerguelen Island 749	Salters et al. (1992)	Basalt	0.30
	Antarctic potential detrital sources		
East Antartica	Sheraton et al. (1992)	Granite	1.19
East Antartica	Sheraton et al. (1992)	Granite	1.12
East Antartica	Sheraton et al. (1992)	Monzonite	1.59
East Antartica	Sheraton et al. (1992)	Quartz-monzonite	2.06

3.2.3. Detrital contents

The detrital fraction (Table 4) of the sediment was estimated from bulk sediment weight minus biogenic components (opal, carbonate, organic matter) with detrital fraction = 1 − (opal fraction + carbonate fraction + 3 × organic carbon fraction).

3.2.4. Biogenic (opal and carbonates) contents

Most of the opal and carbonate (Table 4) data used in this study were previously published by Bareille et al. (1991, 1998). The content of opal was determined by chemical dissolution following the procedure of Mortlock (Mortlock and Froelich, 1989), with resulting uncertainties of less than 2%. The carbonate content (% $CaCO_3$) was determined with a calcimeter by the CO_2 volumetric method. The precision was estimated to be about 2%.

3.2.5. Magnetic susceptibility profiles

Continuous measurements of low-field magnetic susceptibility (MS) were taken on all core samples with a pass-through Bartington magnetometer. This instrument integrates the sediment section within the coil (12.5 cm diameter) with a signal resolution of about 5–10 cm. Down-core integrated MS depends on: (1) the average susceptibility of individual particles; (2) the relative volume of both low (or negative) MS and high MS particles; and (3) the sediment porosity. We used this non-destructive, physical, and extremely rapid method to examine spatial and temporal changes in material input on the southern margin of the SEIR (Bareille et al., 1994).

3.3. Stratigraphic framework and age model

To allow for a more detailed discussion of the signals and their comparison with other records, a chronostratigraphic scale was constructed. Time scales for cores MD 94-102, MD 88-769 and MD 88-770 are based on AMS ^{14}C dates (Labeyrie et al., 1996; Lemoine, 1998). These measurements were obtained from monospecific samples *N. pachyderma* (sin.) at each level. ^{14}C dates were corrected for reservoir age (Bard et al., 1990). For two cores, MD 94-104 and MD 84-552, we have no absolute age constraints. The proposed age scale for these cores was developed as follows:

Core MD 84-552 was correlated graphically to core MD 84-551, which is located in the same area and has age constraints from both $\delta^{18}O$ benthic records and AMS ^{14}C ages (Labracherie et al., 1989). The same procedure was used for core MD 94-104, which was correlated with core MD 88-769.

The results are displayed on an age/depth plot for all the cores (Fig. 3).

4. Results and discussion

4.1. Does long-term current-controlled sedimentation along the SEIR affect climate-driven glacial–interglacial sedimentation?

Current-controlled sedimentation in the SIB has been previously investigated by sediment isopach map (Houtz et al., 1977), seafloor photography, direct current

Table 4
Sediment composition

Core	Depth (cm)	Age (γa)	$CaCO_3$ (%)	Opal (%)	Terrigenous (%)
MD 94-102	0	6.5	68	6	25
	10	8.2	69	6	24
	20	9.9	73	5	21
	30	11.6	79	5	15
	40	13.3	80	5	14
	50	15.0	71	5	24
	60	16.6	67	6	26
	70	17.6	61	7	31
	80	20.7	51	9	40
	90	24.9	48	6	45
	100	29.1	49	6	45
	110	32.6	50	7	43
	120	34.8	52	7	41
	130	35.8	60	7	32
	140	36.8	61	9	30
	150	40.3	66	7	28
	160	43.7	71	5	23
MD 94-104	50	4.3	54	27	20
	100	8.6	62	22	13
	130	11.1	65	15	16
	160	13.0	58	22	26
	180	13.8	49	24	26
	200	14.6	28	22	53
	230	16.0	15	22	66
	300	19.1	15	31	59
	380	22.7	12	27	63
	470	27.5	12	29	58
	600	35.1	21	40	37
	640	37.4	25	38	51
	700	41.0	26	33	48
	800	47.0	25	32	32
MD 88-769	15	8.5	79	7	14
	20	9.7	85	6	9
	25	11.0	83	6	11
	35	13.4	71	9	20
	52	15.7	42	13	44
	64	16.4	25	20	54
	76	17.2	18	22	57
	85	18.0	17	24	57
	95	19.5	16	26	58
	109	21.5	11	28	59
	130	24.2	10	27	62
	149	26.5	17	31	51
	170	29.1	12	28	59

Table 4 (*continued*)

Core	Depth (cm)	Age (γa)	$CaCO_3$ (%)	Opal (%)	Terrigenous (%)
	190	31.7	13	35	50
	210	34.3	25	37	37
	230	36.8	29	33	37
	250	39.6	29	24	45
	270	42.5	25	25	45
MD 88-770	19	7.3	86	6	7
	39	10.2	80	7	13
	49	11.7	80	6	13
	97	16.6	13	50	34
	117	18.2	12	57	28
	159	19.8	10	46	39
	198	21.2	11	57	30
	278	24.6	12	52	34
	339	28.1	12	60	25
	419	34.0	11	63	24
	519	43.2	23	50	25
MD 54-552	19	7.7	25	71	4
	29	8.0	10	87	3
	39	8.3	11	86	4
	49	8.5	9	86	5
	59	8.7	14	83	4
	69	9.3	16	77	7
	77	9.7	14	82	4
	89	10.3	18	79	5
	97	10.7	11	77	13
	109	11.6	8	78	14
	118	12.0	6	81	13
	127	12.3	6	70	23
	139	12.7	8	52	41
	149	13.1	8	47	45
	157	13.9	9	38	56
	169	18.1	9	33	58
	179	20.1	9	38	55
	199	23.9	12	33	56
	219	33.0	15	33	52
	239	41.0	15	42	43

measurements and bottom-water turbidity (Eittreim et al., 1972a; Kolla et al., 1976b, 1978; Kennett and Watkins, 1976). Direct observations of the seafloor and direct current measurements have been used to interpret the accumulation pattern of several million years worth of sediment in the SIB (Kolla et al., 1976b, 1978; Kennett and Watkins, 1976; Houtz et al., 1977). Unfortunately, there is no study available on the glacial–interglacial accumulation pattern.

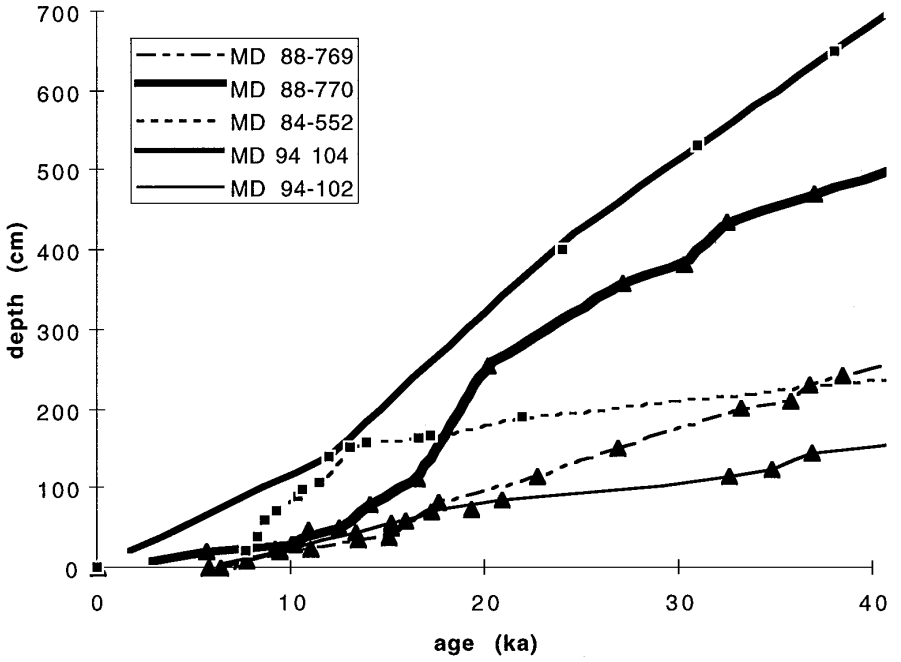

Fig. 3. Stratigraphic results: Age (ka) versus depth (cm). Triangles: Accelerator mass spectrometer ^{14}C dates corrected for reservoir age as proposed by Bard et al. (1990) on planktonic foraminifera (*G. bulloides* and *N. pachyderma s*). Data from Labeyrie et al. (1996) and Lemoine (1998). Squares: Ages derived from different stratigraphic parameters (carbonate, opal, abundance of *Cycladophora davisiana*) by detailed correlation of isotopic stages with cores located in the same area and having age constraints from both $\delta^{18}O$ benthic records and AMS ^{14}C ages.

Before discussing our own geochemical results, in the following sections we will discuss previously published data and will examine glacial–interglacial sedimentation cycles.

4.1.1. The effect of modern currents on the seafloor and long-term sedimentation

The modern northward-moving AABW has widespread effects on sediment transport and accumulation in the western and northwestern part of the SIB, i.e., along the eastern margin of the Kerguelen Plateau and on the southern margin of the SEIR. This influence is determined from the presence or absence of current indicators and manganese nodules on the seafloor of the SIB (Kolla et al., 1976b; Kennett and Watkins, 1976). The strong erosive capacity of intense bottom-water movement in the SIB between 80 and 100°E and 50 and 60°S is revealed by Mn pavement and abundant nodules. This zone is also the location of the lowest sediment thickness (Houtz et al., 1977) (Fig. 4). This correlation suggests that intense bottom currents have persisted in this deep area over 2.5 Ma. This strongly eroded zone has been attributed to the increase in speed of the current as it turns to the east along the

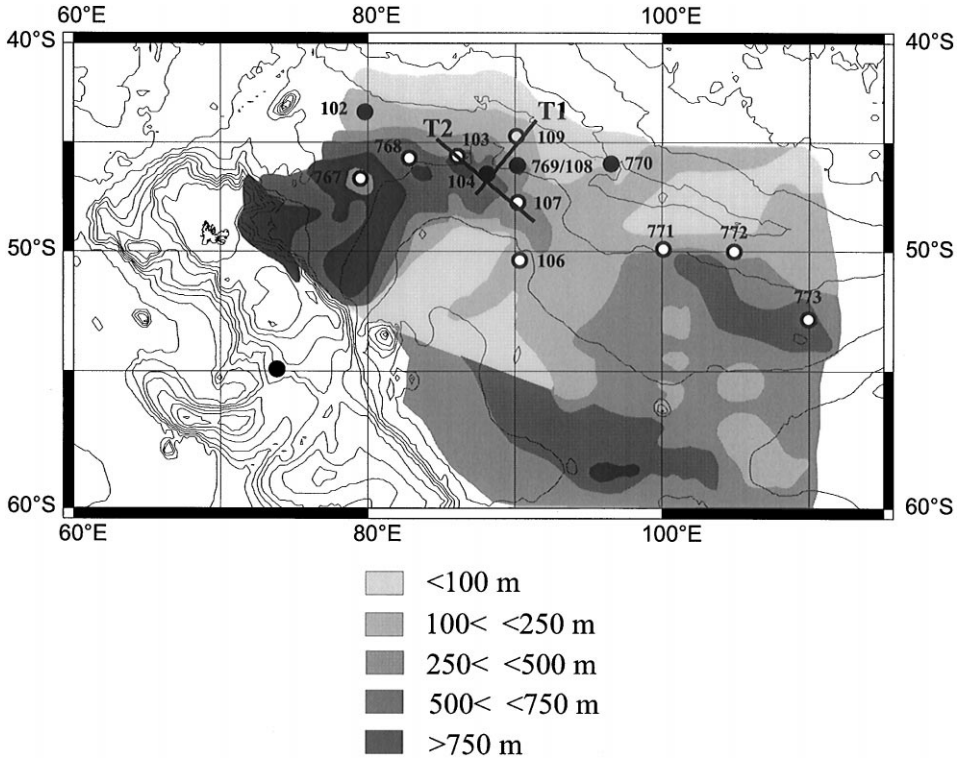

Fig. 4. Sediment thickness (m) inferred from seismic profiles from Eltanin cruises in the Southeast Indian sector of the Southern Ocean (adapted from Houtz et al., 1977). Magnetic suceptibility profiles in Fig. 5 are for the two transects T1 and T2.

southern flank of the SEIR by addition of the high-velocity ACC (Kennett and Watkins, 1976). Strong bottom currents would prevent deposition and result in sediment resuspension, thus generating a large nepheloid layer composed of terrigenous and biogenic particles from bottom sediments (Eittreim et al., 1972a; Kolla et al., 1976b; McCave, 1986; Barron et al., 1991; Ehrmann and Grobe, 1991).

In contrast to the evidence for bottom-water transport and removal of sediments in the zone described above, there is no evidence to suggest any major resuspension from northeast of the Kerguelen Plateau to as far as 110°E (i.e., on the southern flank of the SEIR) from a water depth of 4000 m to the top of the ridge or in the southeastern part of the SIB (south of 56°S). These areas are characterized by relatively high sediment thickness (Fig. 4) and are separated by the low sediment accumulation/high bottom-current zone with Mn pavement to abundant nodules. In the southernmost zone, a sedimentary ridge called the East Kerguelen Ridge (EKR) has been identified along the southern flank of the Kerguelen Plateau. It has been suggested that the EKR could be the product of preferential sediment deposition by the westward-flowing bottom current that is turned northward by the Kerguelen plateau. This suggestion is based

on the combined evidence of a sedimentary ridge (the EKR), the moderate-to-large amount of material in suspension (Kolla et al., 1976b, 1978) and the northward-moving bottom current (Kolla et al., 1976b) along the eastern margin of the plateau (Kolla et al., 1976b; Houtz et al., 1977).

The northern high sediment thickness zone along the southern flank of the SEIR has not been examined in detail. The sediment thickness map of Houtz et al. (1977) suggests the presence of a sediment tongue with sediment thickness decreasing eastwards from the foot of the Kerguelen Plateau. In detail, the pattern of sediment distribution is more complex, with channels of low and high sediment thickness. We suggest that this complexity is due to both topographic effects and bottom-current interactions between the AABW and the ACC, which is strongly concentrated north of the Crozet and Kerguelen Plateaus (Park et al., 1991, 1993). Considering that the sediment tongue probably is the result of millions of years of sedimentation, we selected several Kullenberg cores according to the morphology of the tongue to investigate the last cycle of climate-driven sedimentation on the SEIR (Figs. 2 and 4).

4.1.2. Qualitative evidence of glacial–interglacial current-controlled sedimentation on the SEIR

In the Southern Ocean, glacial–interglacial sedimentary cycles are known to be dominated mainly by substantial amounts of sediment contributed from surface productivity (DeMaster, 1981; Cooke and Hays, 1982). Indeed, material accumulating on the seafloor of the Southern Ocean consists mainly of carbonate oozes north of the Polar Front Zone (PFZ), of silica-dominated oozes between the PFZ and 60°S, and of silty clay or clayey silt (glaciomarine sediments) with varying amounts of biogenic silica between 60°S and the Antarctic continental margin. During glacial periods, the northward migration of the PFZ resulted in the input of detrital material farther north (as far as 42°S) by ice rafting or bottom-current transport (Cooke and Hays, 1982; Howard and Prell, 1992; Bareille et al., 1994). This larger input of detrital material is recorded by an increase in the bulk magnetic susceptibility of glacial sediment intervals (Bareille et al., 1994).

We used this characteristic variability in MS to evaluate the sediment thickness patterns of interglacial and glacial intervals in the sedimentary tongue along the SEIR. Two transects are shown in Fig. 4, one crossing the tongue (T1, Fig. 5a) and the other along the axis of the tongue (T2, Fig. 5b). MS variability suggests that both glacial and interglacial sediment thicknesses follow the millions-of-years sedimentary pattern of the tongue, i.e., higher glacial and interglacial sediment thicknesses are found at the centre and to the west of the sedimentary tongue and decrease eastward, northward and southward from the axis of the tongue. This suggests that late Quaternary sedimentation has been controlled largely by bottom currents in the SIB, despite the input of sedimentary material from surface-water biogenic productivity. Focusing on the Holocene period, additional qualitative evidence for current redistributed sediment on the seafloor comes from the distribution of biogenic silica accumulation rates on the SEIR. Indeed, because biogenic silica production is constrained by frontal zones (PFZ), biogenic silica accumulation rates should be greatest

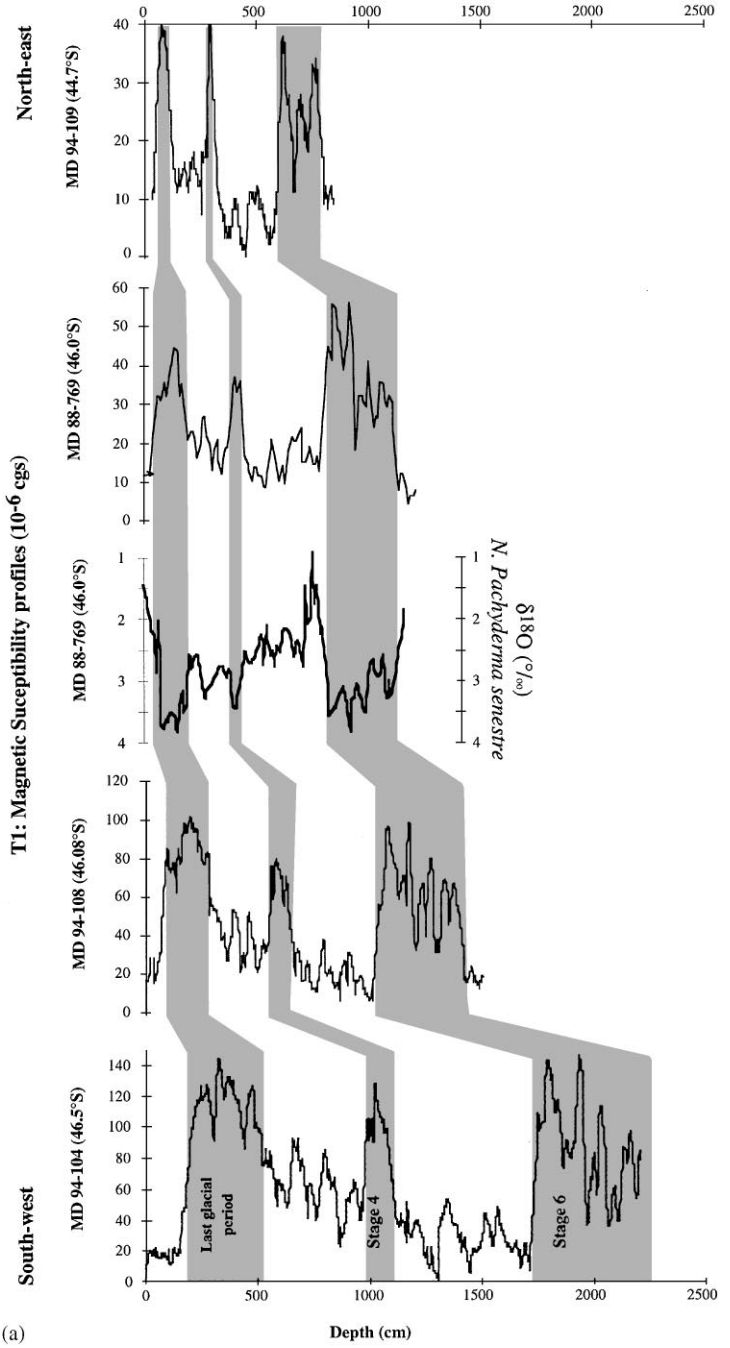

Fig. 5. (a) Magnetic suceptibility profiles versus depth (T1). The $\delta^{18}O$ curve (*N. pachyderma s*) of core MD 88-769 provides a stratigraphic control. (b) Magnetic susceptibility profiles versus depth (T2).

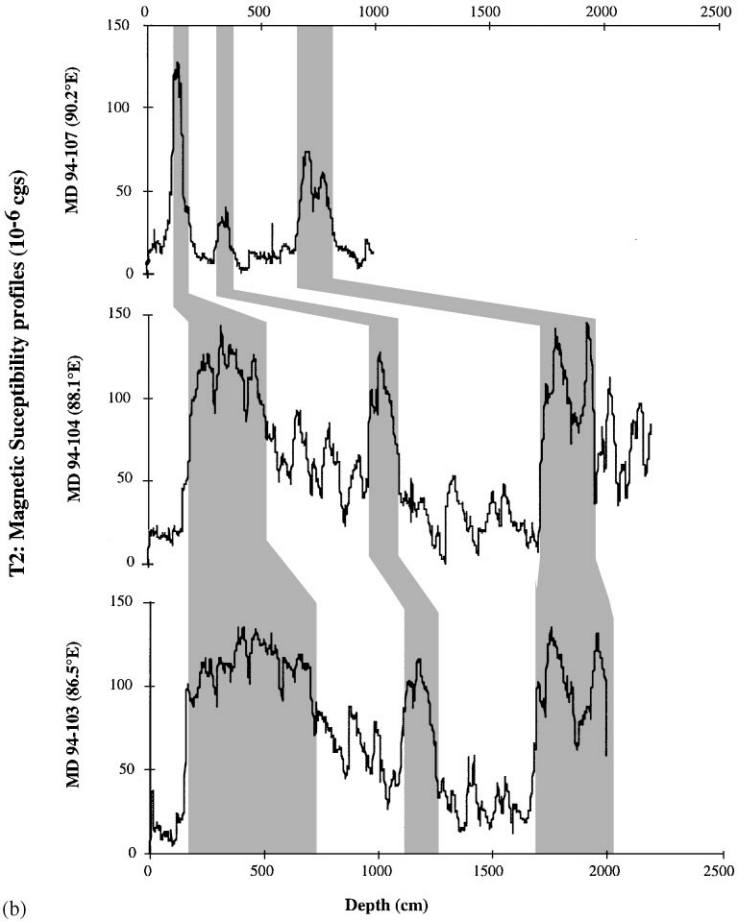

Fig. 5. (*Continued*).

south of the PFZ. However, very high Holocene biogenic silica accumulation rates are found on the SEIR despite their northern location at a distance from the PF (Fig. 6a), highest detrital accumulation rates (Fig. 6b) are also found in this area. In addition, the Holocene distributions of both biogenic silica and detrital accumulation rates (Fig. 6a and b) are in agreement with the eastward trending sediment thickness tongue identified for the long-term sedimentation in the SEIR.

4.2. Quantification of lateral sediment redistribution

As qualitatively shown above, climate-driven biogenic and terrigenous sedimentation in the Southern Ocean should be controlled by the particularly strong bottom-water circulation. A recently developed method, the ^{230}Th normalization

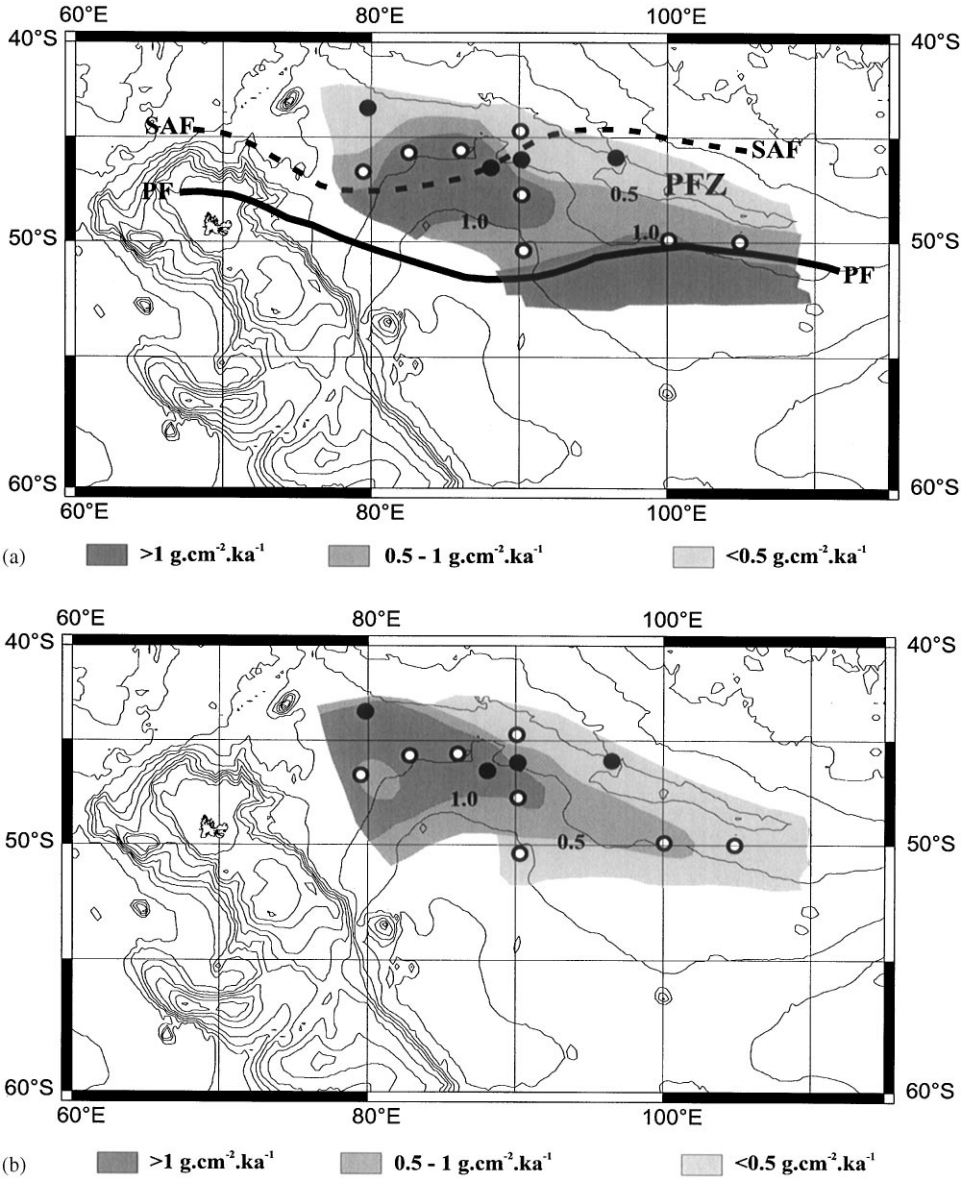

Fig. 6. (a) Biogenic silica accumulation rates for the Holocene period (in g cm^{-2} ka^{-1}). PF: Polar Fronts, SAF: Subantarctic Front; PFZ: Polar Front Zone. (b) Detrital accumulation rates for the Holocene period (in g cm^{-2} ka^{-1}).

flux method (Bacon, 1984; Suman and Bacon, 1989; Francois et al., 1990, 1993; Frank et al., 1995), can be used to identify sections of redistributed sediments and to quantify the amounts of laterally supplied material on the SEIR.

4.2.1. Theory

Thorium-230 is produced at a rate of 2.63×10^{-5} dpm cm^{-3} ka^{-1} in the oceanic water column from the radioactive decay of ^{234}U dissolved in seawater. Because of its long (4×10^5a) residence time in the ocean, uranium concentration in seawater shows no significant geographical variations (Ku et al., 1977). Since Th is strongly adsorbed by marine particulate matter, its residence time in the water column is short (< 40 a, (Moore and Sackett, 1964)), and the rate of ^{230}Th delivery to the sediments is approximately equal to the rate of production, i.e., practically none of the ^{230}Th is lost by decay in the water column. Measurements with deep-sea sediment traps (Anderson et al., 1983) have confirmed that the production and vertical flux of ^{230}Th carried by settling particles are nearly in balance. Thus, ^{230}Th-normalised flux calculations are based on the assumption that the flux of ^{230}Th to the seafloor is constant and equal to its rate of production in the water column (Bacon, 1984; Suman and Bacon, 1989; Francois et al., 1990). In the sediment, this flux constitutes the flux in excess at the time of the deposition, i.e., corrected for the amount of ^{230}Th in the lattice of lithogenic material, for the decay of authigenic uranium, and for the decay of ^{230}Th with time ($^{230}\mathrm{Th}^{\circ}_{ex}$). When lateral sediment redistribution occurs, the flux of $^{230}\mathrm{Th}_{ex}$ into the sediments (F_s) deviates from expected flux value based on the production in the overlying water column (F_w). Suman and Bacon (1989) introduced the focusing factor concept. The focusing factor (Φ) is defined as the ratio of F_s to F_w. $\Phi < 1$ indicates a lateral export of particles loaded with $^{230}\mathrm{Th}_{ex}$ (sediment winnowing) and $\Phi > 1$ indicates, an import (focusing). Thus, average vertical sediment rain rates ($F_{vertical}$) for a certain sediment section may be calculated by dividing the measured sediment accumulation rate F by the F_s/F_w ratio:

$$F_{vertical} = \frac{F}{F_s/F_w} = \frac{F}{\Phi}, \tag{1}$$

where, $F_{vertical}$ is the average vertical sediment rain rate for an independently dated section (g cm^{-2} ka^{-1}); F is the accumulation rate (g cm^{-2} ka^{-1}); F_s is the flux or accumulation rate of $^{230}\mathrm{Th}^{\circ}_{ex}$ (dpm cm^{-2} ka^{-1}):

$$F_s = C_{(x)} S \,\mathrm{DBD},$$

where $C_{(x)}$ is the concentration (decay-corrected) of $^{230}\mathrm{Th}_{ex}$ ($^{230}\mathrm{Th}^{\circ}_{ex}$) at the depth x in the sediment, S is the sedimentation rate (cm ka^{-1}), and DBD is the Dry Bulk Density (g cm^{-3}); and F_w is the constant production rate of ^{230}Th in the water column (dpm cm^{-2} ka^{-1}):

$$F_w = \beta Z,$$

where Z is the water depth (cm) at the core location and β is the production rate of ^{230}Th in the water column (2.63×10^{-5} dpm cm^{-3}ka^{-1}).

This approach was successfully applied in localities where lateral re-sedimentation is significant (Suman and Bacon, 1989; Francois et al., 1993).

4.2.2. Calculating age-corrected excess ^{230}Th activity at the time of deposition

There are two prerequisites for utilization of ^{230}Th data to determine accumulation fluxes. Firstly, the measured concentrations of ^{230}Th have to be corrected for both detrital and authigenic contributions produced from decay of ^{234}U in the sediment in order to calculate the amount of ^{230}Th originating from scavenging in the oceanic water column (excess concentrations). Secondly, an independent time-scale for the core is necessary to calculate the corresponding value at the time of deposition ($^{230}\mathrm{Th}^{\circ}_{ex}$) for each measured $^{230}\mathrm{Th}_{ex}$ content.

4.2.2.1. Evaluation of detrital and authigenic ^{238}U activities. The total 238 uranium measured in the samples consists of two components: uranium present in detrital minerals ($^{238}\mathrm{U}_d$) and bio-authigenic uranium ($^{238}\mathrm{U}_{ba}$) derived from seawater.

Detrital uranium ($^{238}\mathrm{U}_d$) is estimated as

$$^{238}\mathrm{U}_d = (^{238}\mathrm{U}/^{232}\mathrm{Th})_d(^{232}\mathrm{Th})_s,$$

where $(^{238}\mathrm{U}/^{232}\mathrm{Th})_d$ is the detrital U/Th ratio and $(^{232}\mathrm{Th})_s$ is the measured content of ^{232}Th in the sediment samples. ^{232}Th is considered to be present exclusively present in detrital minerals (Anderson, 1982).

The bio-authigenic uranium ($^{238}\mathrm{U}_{ba}$) contents of the samples were then calculated:

$$^{238}\mathrm{U}_{ba} = {}^{238}\mathrm{U}_T - {}^{238}\mathrm{U}_d,$$

where $^{238}\mathrm{U}_T$ is the measured total uranium content.

In core MD 94-102, the good correlation of ^{232}Th with $^{238}\mathrm{U}_T$ ($r^2 = 0.8$) suggests that bio-authigenic uranium is not present. The detrital $(^{238}\mathrm{U}/^{232}\mathrm{Th})_d$ ratio of 0.58 from this core is applied to the calculations for all cores in the study area.

In order to calculate the activities of detrital and bio-authigenic uranium, Francois et al. (1993) assumed a $(^{238}\mathrm{U}/^{232}\mathrm{Th})_d$ activity ratio of the detrital sediment phase in the range of 0.5–1, and Frank, 1996 used an activity ratio of 0.75. Our U/Th ratio is within the range used in these previous studies.

4.2.2.2. Age-corrected excess ^{230}Th activity. The following equations are applied to calculate the age-corrected excess ^{230}Th activity ($^{230}\mathrm{Th}^{\circ}_{ex}$):

$$^{230}\mathrm{Th}_{ex} = {}^{230}\mathrm{Th}_{meas.} - (^{232}\mathrm{Th} \times 0.58) - {}^{238}\mathrm{U}_{auth.} \times [(1 - e^{-\lambda_{230}t}) + \lambda_{230}/(\lambda_{230} - \lambda_{234}) \times (1 - e^{-(\lambda_{230} - \lambda_{234})t})((^{234}\mathrm{U}/^{238}\mathrm{U}) - 1)],$$

where

$$^{238}\mathrm{U}_{auth.} = {}^{238}\mathrm{U}_{meas.} - (^{232}\mathrm{Th} \times 0.58)$$

with $(^{232}\mathrm{Th} \times 0.58)$ being the estimate of the mean activity of detrital ^{238}U in dpm g^{-1}, λ_{230} and λ_{234} are the decay constants of ^{230}Th and ^{234}U in a^{-1}, and t is the age in years estimated from previous stratigraphic results.

The $^{238}\mathrm{U}_{auth.}$ term represents the equilibrium activity of ^{230}Th produced from authigenic uranium, assuming that uranium precipitation occurred at the time of sediment deposition. After the stratigraphy is established, the excess activities of the

radionuclides are decay-corrected to the time of deposition of the sediment ($^{230}Th^{\circ}_{ex}$):

$$^{230}Th^{\circ}_{ex} = {}^{230}Th_{ex}\, e^{\lambda t}.$$

Measured age-corrected $^{230}Th_{ex}$ activities are shown in Table 2. These activities show small fluctuations in most of the cores investigated from the SEIR and the Kerguelen Plateau.

4.2.3. Fluxes estimated by the $^{230}Th^{\circ}_{ex}$ method compared with accumulation fluxes

When comparing the sediment accumulation rates to the vertical particle rain rate calculated by the constant $^{230}Th^{\circ}_{ex}$ accumulation method (Eq. (1)), we note dramatic differences between the two records for all deep-sea cores (Fig. 7).

In the northwestern part of the SIB and in the plateau area, the sediment accumulation rates are several times higher than our estimated rain rates throughout the investigated period of time (approximately 2–14 times higher). This confirms our initial assumption about anomalies of high accumulation of biogenic silica in the PFZ along the SEIR during the Holocene period.

In order to facilitate a more convenient core-to-core comparison, we used the focusing factor concept introduced by Suman and Bacon (1989). There are, however, several assumptions and problems that lead to uncertainties in calculating the focusing factor. Having demonstrated that these problems are negligible for our cores (see appendix), we present a map showing F_s/F_w ratios in two time slices in order to see if any systematic links to paleoclimate-driven changes of the current regime can be recognized.

4.2.3.1. The Holocene. The Holocene (here 0–13 ka BP) redistribution map (Fig. 8a) shows that all sites are affected by sediment focusing. Application of Eq. (2) indicates that the amount of $^{230}Th^{\circ}_{ex}$ that accumulated at the coring location exceeded that which was produced in the overlying water column by a factor of 3–5 and by as much a factor of 9 in core MD 94-104 located just east of Kerguelen Island, and a factor of 10 in core MD 84-527 located just northeast of Crozet Plateau.

In comparing the sediment distribution map reconstructed from seismic profiles to the geographic pattern of focusing factor, we observe a general correspondence between high thickness and Φ, suggesting a strong link between circulation and laterally supplied material.

4.2.3.2. Isotope stage 2. The pattern for the last glacial period is not very different from the pattern for the Holocene except that a stronger lateral contribution of sediment (i.e., higher values of Φ) can be observed along the base of the SEIR (Fig. 8b). Compared with the Holocene period, the focusing factor is clearly above 4 in cores MD 88-769 and MD 88-770 during stage 2, and is up to a factor of 12 in core MD 94-104. On the northern slope of the Crozet Plateau (MD 84-527), the focusing factor is below 1, suggesting a weak winnowing, which means that an export of particles, probably due to increased bottom-current velocities, occurred.

Although the patterns of sediment dispersal and accumulation are similar for glacial and interglacial times, there are significant differences in the quantity of material

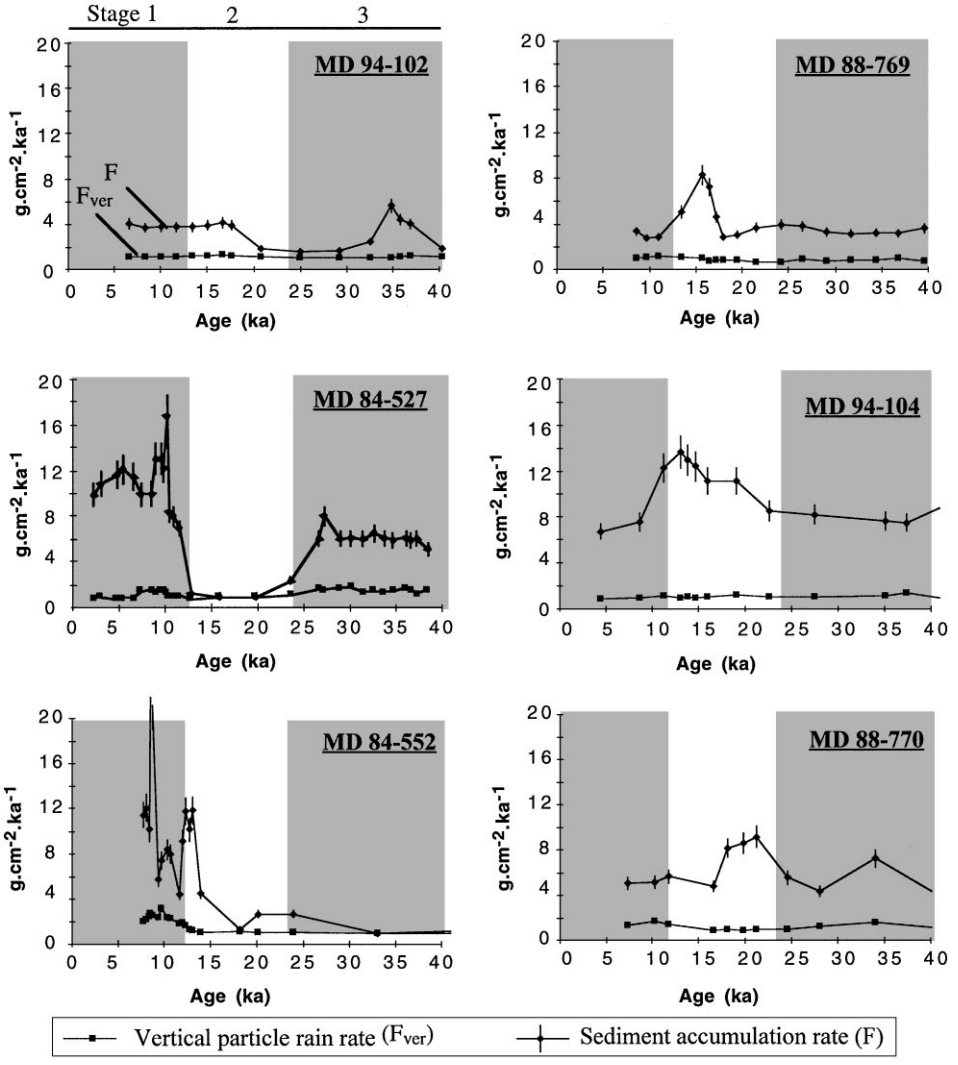

Fig. 7. Vertical particle rain rate estimated by $^{230}Th_{ex}$ method compared with sediment accumulation rate. Core MD 84-527 has been previously studied by François et al. (1992).

advected. These differences are quite clear and must reflect a change in the position or intensity of the bottom currents of the AABW or ACC-CDW, which are believed to be the agent that delivers sediment to the sites. So, it is interesting to note that the mapping of the focusing factor data shows dynamic erosion of the northern slope of the Crozet Plateau and an increasing lateral supply of sediment to the base of the SEIR during the glacial period. A preliminary interpretation of this pattern is that near the present-day location of the SAF, there has been a significant hydrographic

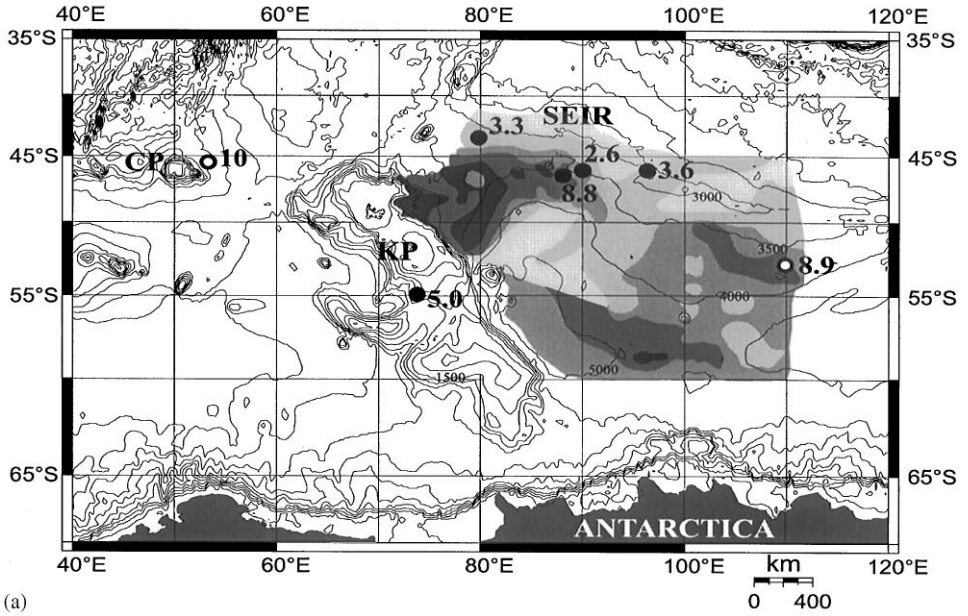

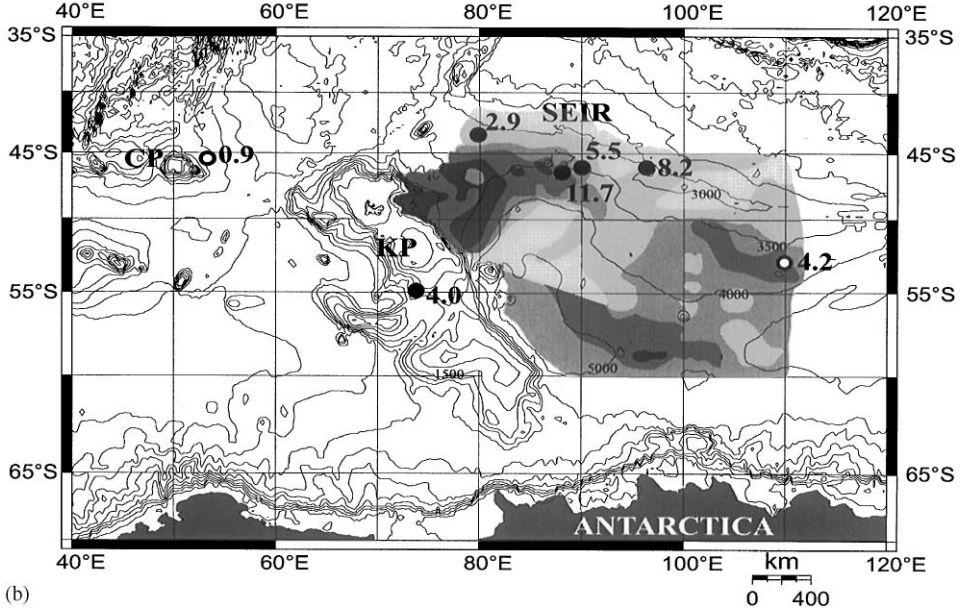

Fig. 8. (a) Distribution of the focusing factor (Φ) for the Holocene period superimposed on thickness variations (Fig. 4). CP: Crozet Plateau; KP: Kerguelen Plateau; SEIR: Southeast Indian Ridge. (b) Distribution of the focusing factor (Φ) for the glacial period superimposed on thickness variations (Fig. 4).

change between the last glacial conditions and those now prevalent during the Holocene. This change in conditions may be related to a higher flow speed of the ACC-CDW during the glacial period in comparison with the Holocene. However, a major contribution of Antarctic material transported by enhanced AABW during the glacial period cannot be ruled out. Consequently, we investigated the origin of glacial lateral inputs.

4.3. Detrital input

To the east of Kerguelen, Copin-Montegut and Copin-Montegut (1978) noticed an increase (approximately double) in particulate silica with depth in the water column. This increase has been attributed to the resuspension of bottom sediment rich in siliceous tests by bottom water. The increase in Si is accompanied by an increase in Al, Fe and Mg, showing that significant amounts of terrigenous material are also brought into suspension. The application of the $^{230}Th^{\circ}_{ex}$ method provides evidence for significant biogenous and terrigenous sediment redistribution during the last 40 ka. These results raise questions about the origin and the mode of transport of this material. Here, we propose an original approach to this question by identifying the origin of particles and the variations in their composition as a function of time. Terrigenous particle origin can be determined by using rare-earth elements (REE) and other trace elements.

4.3.1. Rare-earth elements and other trace elements

In the northwestern part of the SIB, terrigenous particles may originate from any of the surrounding land masses, i.e., old Antarctic continental craton and volcanic oceanic islands (Kerguelen, Crozet). These potential source areas are characterized by different REE or trace-element compositions. Thus, by connecting the REE or trace-element composition of source areas to the terrigenous particles in the sediment, the origin of the particles can be identified. In order to characterize the spatial and temporal changes in detrital fluxes during that last 40,000 yr, we chose to focus on three cores (MD 94-102, MD 88-769 and MD 94-104) selected from the contourite drift.

4.3.1.1. Rare-earth elements. In order to obtain the best resolution in this identification, we chose to use the degree of light REE enrichment with respect to heavy, REE, which discriminates between the two potential source areas and is defined as:

$$La_n/Tb_n = (La_{sample}/La_{shale})/(Tb_{sample}/Tb_{shale}).$$

The old Antarctic continental craton is characterized by La_n/Tb_n ratio above 1.00 and the young volcanic islands (Crozet, Kerguelen) by a ratio under 0.90 (Table 3). The lithogenic signal of the bulk sediment may be altered by biogenous skeletal materials and by a hydrogenous-hydrothermal signal. Elderfield et al. (1981) showed that the direct contribution of plankton and carbonate and siliceous skeletal materials to REE contents of sediments is negligible. In the cores from this study, the contribution of La and Tb from biogenous material is negligible ($<10\%$) when the biogenous material

constitutes less than 80% of the bulk sediment. Samples of cores MD 88-769 and MD 94-104 have biogenous material contents greater than 80% during the Holocene. In order to determine the Holocene lithogenic characteristics at these sites, we carried out measurements on carbonate-free fractions. Core MD 94-102 has biogenous material contents of less than 80%, permitting reasonably accurate determinations of the Holocene lithogenic characteristics at this site.

The lithogenic signal may also be altered by a hydrogenous-hydrothermal signal in coatings of oxide hydroxide on the grains analysed (Elderfield et al., 1981; Palmer, 1985). However, REE analyses of the samples revealed no significant cerium anomaly, the latter being expected in the case of a hydrothermal component, ferromanganese nodules or diagenetic products associated with an authigenic Fe–Mn-rich phase adsorbed onto surface of particles. The Fe/Se ratio is constant for all cores, with a value around 3.4 ($r^2 = 0.98$), which signifies a detrital rather than authigenic origin for Fe. Moreover, the accumulation rates in that area are too high to permit an increased Fe–Mn-rich phase. Consequently, we assume that the geochemical composition of our samples is more likely to represent the lithogenic signal. The La_n/Tb_n and Fe/Sc ratios of the sediments from the cores are shown in Table 3.

The measured La_n/Tb_n ratio (Fig. 9a) clearly shows a change in terrigenous origin between the glacial period and the Holocene. Samples representing glacial stages 2 and 3 reveal lower La_n/Tb_n ratios compared with those from the Holocene. Although the variations are small, La_n/Tb_n ratios are well above 0.8 during the Holocene, indicating a higher relative contribution of terrigenous particles from the Antarctic source than the volcanic source at this time. These ratios were lower during the glacial period, indicating a likely relative increase in the volcanic contribution.

4.3.1.2. Other trace elements. In addition to the La/Tb ratio, we also considered the distribution of Th and Sc for the purpose of determining the origin of detrital particles. Both strongly incompatible elements (like Th) and strongly compatible elements (like Sc) are present in clastic sedimentary rocks (Taylor and McLennan, 1985). Their ratios provide an index of chemical differentiation (e.g., Th/Sc) and may provide a sensitive index of overall chemical composition (i.e., mafic versus felsic). A lower Th/Sc ratio in sediments could reflect a higher proportion of detrital particles derived from oceanic crust (e.g., Kerguelen, Crozet). The advantage of the Th/Sc ratio over the La_n/Tb_n ratio is that the lithogenic signal of the bulk sediment is not altered by biogenous skeletal materials or by a hydrogenous-hydrothermal signal. The Th/Sc ratios are shown in Table 3 and Fig. 9b.

The measured Th/Sc ratios (Fig. 9b) differ between interglacial and glacial periods. These variations in Th/Sc ratios are interpreted to indicate a change in the origin of the detrital material. Samples from cores representing glacial stages 2 and 3 have lower Th/Sc ratios than those from the Holocene, with values ranging from 0.3 to 0.4. As volcanic rocks from Kerguelen have Th/Sc ratios ranging from 0.01 to 0.4 (Storey et al., 1988), and as the Th/Sc ratio of core MD 84-552 is constant (0.35) for both glacial and interglacial periods, the Th/Sc ratio in sediments at the base of the SEIR

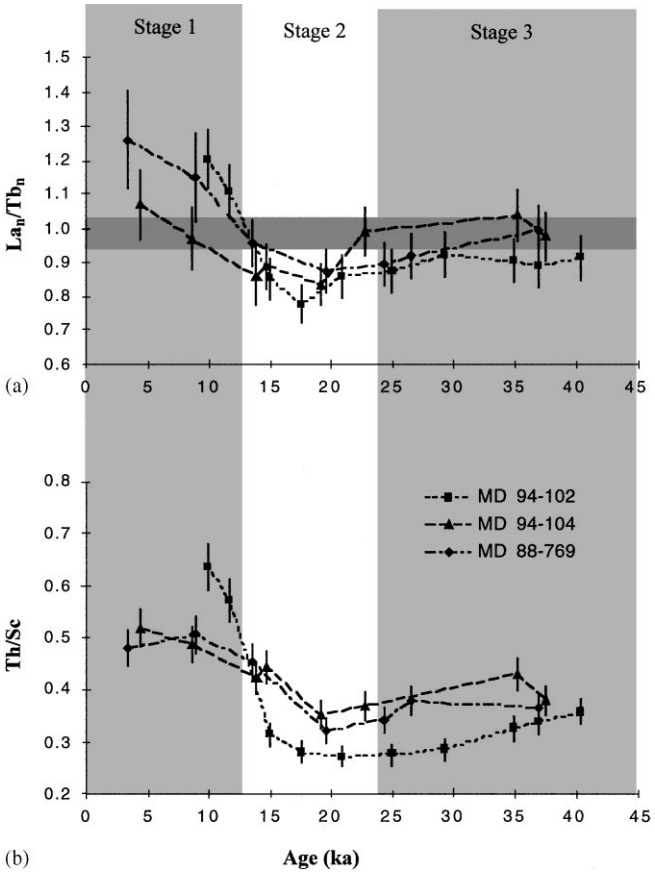

Fig. 9. Downcore evolution of La_n/Tb_n and Th/Sc ratio in the cores MD 94-102, MD 94-104 and MD 88-769.

supports enhanced material coming from the Crozet-Kerguelen sources during glacial times.

The La_n/Tb_n and Th/Sc ratio data suggest that during the last 40 ka, the terrigenous particles originated from two major sources: the volcanic oceanic islands (Kerguelen, Crozet), consistent with the action of a bottom water mass (i.e., ACC-CDW) flowing from the volcanogenic islands into the SIB, or the old Antarctic continental craton, consistent with the action of a bottom water mass (i.e. AABW) flowing from the Antarctic continent into the SIB. The lower La_n/Tb_n and Th/Sc ratio during the glacial period might be related to greater volcanic inputs because of increased erosive capacity of the ACC-CDW due to its higher speed during this period. The increase of these ratios in the Holocene suggests less ACC-supplied material of Crozet and Kerguelen origin.

4.3.2. Sediment supply and transport mechanisms

The main question remaining to be addressed pertains to the increase in the glacial detrital flux: does this increase reflect a change in bottom-current strength or a change in transport mechanisms?

The detrital fraction can be transported into the ocean by wind (aeolian particles), by surface circulation (ice-rafted detritus), by turbidity currents and by bottom currents. Our interpretation of geochemical and focusing data is that deep-current transport is the likely explanation for detrital flux into the basin. However, the possibility of contributions of detrital material transported by these other means has not been discussed. We here investigate the input of sediment via different transport mechanisms and demonstrate that their contributions to the detrital sediment flux in the SEIR are negligible.

4.3.2.1. Aeolian input. Grousset et al. (1992) showed that dust from the last glacial maximum found in East Antarctica at Dome C came mostly from Argentine loesses (Patagonia). These dusts are therefore likely to have an old continental cratonic signature. In oceanic sediments, however, the detrital fraction accumulated on the SEIR commonly consists of volcanic material. In addition, Duce and Tindale (1991) showed modern aeolian fluxes of 0.001–0.01 g cm^{-2} ka^{-1} for the Southern Ocean. Assuming that Vostok dust flux was greater by a factor of 15 during the last glacial maximum (Petit et al., 1990), glacial dust flux to the Southern Ocean would be about 0.015–0.15 g cm^{-2} ka^{-1}, representing less than 5% of the total detrital flux of the southeast Indian sector. We thus exclude aeolian input as a main transport mechanism of detrital sediments to the basin.

4.3.2.2. Ice-rafted detritus supply. Higher detrital input during glacial periods could potentially be explained by greater input of ice-rafted detritus. In the Atlantic sector of the Southern Ocean, Cooke and Hays (1982) showed a higher IRD input during glacial periods with a decreasing gradient from the Weddell sea to the Indian Basin. On the other hand, evidence for input of iceberg melt water in the surface waters of the Antarctic polar front has been clearly identified in $\delta^{18}O$ anomalies in the Atlantic and the western sector of the Indian Basin (Labeyrie et al., 1986). No anomaly due to input of iceberg melt water in the surface waters was identified in the eastern sector, i.e., from the Kerguelen Plateau to the SEIR (cores MD 80-304, RC 11-120, MD 88-769, MD 88-770, MD 94-102 (Labeyrie et al., 1986, 1996; Lemoine, 1998)).

Ice rafting is an important delivery mechanism if the terrigenous sediment flux has a tremendous control over vertical rain rates. We have determined the vertical rain rates and the detrital particle fluxes for our cores and can show that variations in the bulk accumulation rain rates are not correlated with the detrital rain rates (MD 94-102 ($r^2=0.09$), MD 94-104 ($r^2=0.05$), MD 88-769 ($r^2=0.30$), MD 88-770 ($r^2=0.18$), MD 84-527 ($r^2=0.10$). Moreover, a high-resolution time study in MD 88-769 has been carried out by Manthe and Bareille (2000) in order to identify and separate the ice-rafted sediment contribution. They showed that most of terrigenous debris deposited in the sediment accumulation band is relatively fine and that the fraction >45 μm (which may be considered as ice-rafted detritus) represented less

than 5% during glacial periods. Ice rafting is therefore unlikely to be a major transport mechanism for detrital sediment on the SEIR.

4.3.2.3. Turbidity current processes. During glacial periods, as a result of lower sea level, shelves and shallow plateaus may be destabilized. Compared with the interglacial periods, when most of the detrital particles were trapped on the shelves, during glacial periods, sediments may be transported to the deep sea by turbidity currents or slumping. The only likely source of turbidities is Kerguelen Plateau, and the sediment body cored lies on the flank of the SEIR, separated from Kerguelen by a depression that would take turbidity currents down into the SIB. They are most unlikely to have been direct supplies of material. Moreover, in the case of strong turbidity currents during glacial periods, ^{14}C age-inverted sections are expected, but not observed, in our cores.

4.4. Paleoceanographic implications

4.4.1. Bottom-current variability in the Indian sector of the Southern Ocean

Physical (magnetic susceptibility profiles), sedimentological (detrital and opal contents) and geochemical ($^{230}Th_{ex}^{\circ}$, REEs and trace elements) results suggest that changes occurring in the accumulation pattern on the southern flank of the SEIR during the last 40 ka were derived mainly from the decreased supply of advected material from glacial to Holocene. We believe that this change is related to changes in the interactions between the ACC-CDW and the AABW.

During the Holocene epoch, the detrital material supplied to the SEIR clearly shows a mixed continental (the Antarctic craton) and volcanic (Kerguelen Plateau) origin. This mixed origin suggests that the detritus was transported in suspension by deep-water currents along both Antarctica and the Kerguelen plateau. Large inputs of biogenic silica were also found in the same area as evidenced by comparison of vertical rain rates and accumulation rates in sediments. This is also supported by the presence of Antarctic diatom species (L. Armand, personal communication, 1999) along the Kerguelen plateau. Thus, there is new evidence supporting the interpretation that significant amounts of biogenous and terrigenous material are brought into suspension by the bottom nepheloid layer (northward-moving AABW), as previously stated by Kennett and Watkins (1975, 1976).

During the glacial periods, both detrital and biogenic silica fluxes of advected origin were higher than in the Holocene on the SEIR. Enhancement of volcanic material input relative to that from the Antarctic continental source supports the idea of resuspension processes and transport by deep-water currents along the northern part of the Kerguelen Plateau. Focusing factor data show dynamic erosion of the northern slope of the Crozet Plateau, confirming this assumption. This source of terrigenous material is consistent with the action of stronger bottom-water currents associated with the ACC-CDW flowing eastward from the Crozet and Kerguelen Plateaus during the glacial period, as stated by a simple wind-driven model (Klinck and Smith, 1993). Concerning the source of biogenic silica, a portion could be associated with the dispersal of local productivity as the PFZ moved to the north during the glacial

periods, and some is likely to originate from the northern slopes of the Crozet and possibly Kerguelen plateaus, as suggested by the occurrence of winnowing processes in these areas. Taking into account the main terrigenous source, this latter source should be of greater importance. Consequently, we believe that increasing lateral supply at the foot of the SEIR during the glacial period comes from sediment resuspension from the north slopes of Crozet and Kerguelen plateaus, just west of the coring locations. This interpretation is consistent with hydrographic data from the region (Park et al., 1991, 1993), indicating that the northward deflection of the circumpolar current results in relatively strong eastward currents that could scour the northern slope of the plateau. There is some evidence for rather low bottom-water current velocities associated with the AABW during glacial periods. For example, velocity estimates obtained in the Weddell Sea suggest that during the coldest periods, when sea ice cover was more extensive than today, bottom currents were weaker (Pudsey, 1992). A similar conclusion has been made for the North Atlantic Deep Water (Duplessy et al., 1988). Ehrmann and Grobe (1991) found cyclic changes in Pleistocene sedimentation from the East Kerguelen Ridge, a contourite ridge associated with the AABW movement along the eastern flank of the Kerguelen plateau (sites 745 and 746, ODP leg 119). On this contourite, facies rich in biogenic silica alternate with clay-siliceous facies; these facies are associated with interglacial and glacial periods, respectively. Glacial periods are characterized by lower sedimentation rates that could be interpreted as resulting from a decrease in the deposition of material. This decrease could result from a weaker current, or from higher current velocities inhibiting sedimentation. In the latter case, we would find evidence for erosion on the East Kerguelen Ridge, but we have no indication of such a process. On the other hand, the material should be deposited in a northern location like the SEIR, but we have not found clear evidence of higher quantities of material from Antarctica. This suggests that the AABW circulation was not significantly different than today and may have been less erosive in the southeast Indian basin during glacial periods than during interglacial times as stated by Ehrmann and Grobe (1991). Consequently, an enhancement in bottom-water current strength associated with the ACC-CDW seems to be the principal factor causing more significant transfer of terrigenous products to the contourite drift.

Because of its close relation to wind stress, the ACC could have changed in strength in response to wind stress changes. Micropaleontological reconstructions of sea surface temperature in the SW Indian Ocean during the last glacial maximum (LGM) suggest a northward migration in the position of the Subtropical Front (STF) and the Polar Front (PF) (Labeyrie et al., 1996; Lemoine, 1998). The foraminiferal record also suggests that the PF migrated more than the STF, resulting in a contraction of the Polar Frontal Zone during the LGM. In that case, an increase in speed of the ACC-CDW may also have been induced by an increase in the meridional density gradient.

4.4.2. The contourite formation along the SEIR during the glacial period

Currents causing contourite formation must be slow enough to allow the accumulation of suspended material. One ambiguity comes from the fact that in our hypothesis,

glacial increase in ACC-CDW would probably not create conditions to deposit larger quantities of material on the ridge.

During the glacial period a combination of increased wind stress and contraction of the Polar Frontal Zone results in faster flow of the ACC-CDW. The currents associated with the ACC-CDW are accelerated around the north end of major obstructions presented by Crozet and Kerguelen plateaus. The higher erosive capacity of these currents along the northern slopes of these plateaus could generate a larger nepheloid layer which incorporated terrigenous and biogenous particles from bottom sediments. Downstream of Kerguelen a decrease of the topographic control induced a decrease of the bottom-current intensity and resulted in the sedimentation of most of the particle load of the CDW against the SEIR.

5. Conclusion

Sediment redistribution over the last 40 ka by bottom currents has been investigated using a suite of cores obtained from three distinct environments. These environments are: the eastern part of the Crozet Islands (MD 84-527), the western part of the Kerguelen plateau (MD 84-552) and the northwestern part of the SIB (MD 94-102, MD 94-104, MD 94-106, MD 88-769, MD 88-770). Sediment thickness distribution, magnetic susceptibility profiles, detrital and opal contents, $^{230}Th^{\circ}_{ex}$, REE and trace-element analyses have permitted several conclusions to be drawn:

(1) Dramatic changes in accumulation rates of sediments recorded in cores were caused principally by changes in lateral transport by bottom currents rather than by changes in aeolian or IRD particles settling from the overlying water column or turbidity current supply.

(2) The La_n/Tb_n and Th/Sc ratio data revealed that during last glacial period, the terrigenous particle source was mainly of volcanogenic origin, i.e., the Crozet and Kerguelen slopes. The more significant contribution from the volcanic sources during the last glacial maximum is consistent with the more vigorous action of ACC-CDW bottom water mass. Moreover, mapping of the focusing factor data shows dynamic erosion ($\Phi < 1$) of the northern slope of the Crozet Plateau and an increased lateral supply ($\Phi > 1$) at the foot of the Southeastern Indian ridge during the glacial period. A preliminary interpretation of this pattern is that there was a significant hydrographic change from the last glacial period to the Holocene around the present-day location of the SAF, which might be related to an increase in speed of the ACC-CDW.

(3) To explain the contourite drift formation along the SEIR, we propose that sediment that was eroded by high bottom-water velocities associated with the ACC-CDW was deposited in a region of lower current intensity on the SEIR. The expansion of the Polar Frontal Zone to the east of the Kerguelen Plateau, the lesser topographic control and the confluence of the ACC-CDW with the northward flowing AABW, would have induced a decrease in the circumpolar current velocity along the southern flank of the SEIR, thus allowing the deposition of suspended material.

In summary, the combined sedimentologic, seismic and geochemical approaches used in this study have permitted us to understand the functioning of the basin. These approaches hold great potential for study of oceanic sedimentation processes with implications for paleocirculation.

Acknowledgements

This research was supported in part by the CNRS, the CEA and the French Institut des Sciences de l'Univers. We thank M. Truffy and M. Bonté (LSCE, France), who helped us with trace-element analyses by neutron activation. Piston cores were recovered during the "APSARA II (1984), APSARA IV (1988)" and "PACIMA (1994)" cruises: we are most grateful to the officers and crew of the R/V *Marion-Dufresne*. These cruises were funded by the Territoires et Terres Australes et Antarctiques Françaises (TAAF).

Appendix A

There are several assumptions and problems that lead to uncertainties in calculating the focusing factor.

(1) The first assumption is that lateral isopycnal transport of dissolved ^{230}Th within the water column (boundary scavenging) from high to low particle flux areas, is negligible. This boundary scavenging occurs when marginal sediments receive a much greater flux of particle-reactive elements than open ocean sediments. An increased lateral transport of isotopes along isopycnals should result in increased radionuclide fluxes to the sediment and should coincide with increased sedimentation rates. On the other hand, a lateral isopycnal export of radionuclides should coincide with decreased radionuclide fluxes and decreased sedimentation rates. In this study, cores have higher $^{230}Th_{ex}^{\circ}$ fluxes (F_s) than the ^{230}Th production flux (F_w). So, an increased amount of "boundary scavenging" due to a higher particle rain rate could explain the high ^{230}Th fluxes. However, several lines of evidence suggest that this effect is unimportant for our cores, Firstly, the $^{231}Pa_{ex}^{\circ}/^{230}Th_{ex}^{\circ}$ ratio may be an indicator of biologically induced scavenging Because it has a longer residence time in sea water, $^{231}Pa_{ex}$ is preferentially scavenged in high-flux regions (Anderson et al., 1990), where settling materials and underlying sediments acquire a $^{231}Pa_{ex}^{\circ}/^{230}Th_{ex}^{\circ}$ ratio higher than their production-rate ratio from the decay of uranium dissolved in sea water (0.093). In contrast, sediments deposited in low-flux regions have a $^{231}Pa_{ex}$ deficit (that is, $^{231}Pa_{ex}^{\circ}/^{230}Th_{ex}^{\circ} < 0.093$). Walter et al. (1997) recently reported that the relationship between $^{231}Pa_{ex}^{\circ}/^{230}Th_{ex}^{\circ}$ and particle flux was more complex and suggested that $^{231}Pa_{ex}^{\circ}/^{230}Th_{ex}^{\circ}$ ratios responded more to the rain rate of opal than to the total flux of particulate matter sinking through the water column. Francois et al. (1997) used the ratio $^{231}Pa_{ex}^{\circ}/^{230}Th_{ex}^{\circ}$ in order to study past changes in opal fluxes in the Southern Ocean. Their results clearly give evidence that little glacial-to-Holocene change occurs

in the Indian sector, suggesting a constant opal rain rate throughout the investigated time period. They also suggest that biologically induced scavenging was not very strong ($^{231}Pa^{\circ}_{ex}/^{230}Th^{\circ}_{ex}$ ratio not far from the production-rate ratio). Secondly, in different oceanic regions, Francois et al. (1990) showed that while total mass flux collected by the traps varies 15-fold between low- and high-productivity regions, the accompanying flux of ^{230}Th varies from a deficit (compared to ^{230}Th production rate) of circa 40% in oligotrophic regions to a maximum excess of circa 50% in high-flux areas. In the extreme case, if we assume strong upwelling and a high mass flux in our study, then the $^{230}Th_{ex}$ flux would be increased by a factor of 2 by boundary scavenging. In that case, only a focusing factor above 2 may then be interpreted as sediment redistribution.

For the above reasons, the higher glacial $^{230}Th^{\circ}_{ex}$ fluxes (F_s), which may be up to 14-fold the ^{230}Th production flux (F_w), cannot be due to increased scavenging by changes in particle rain rate (Fig. 7).

(2) The second assumption that has to be made for estimation of the focusing factor (Φ) is that the ^{230}Th concentration in the redistributed sediment is equal to that of the sediment raining down from the overlying water column (i.e., if the redeposited sediment came from an area of similar water depth). As suggested by Francois et al. (1993), it is also possible that the redistributed sediment was initially deposited at a shallower depth prior to being transported to its final site of deposition. In this case, Φ would underestimate the fraction of sediment brought by lateral transport and vertical paleofluxes would overestimate true rain rates. However, several lines of evidence suggest that this problem is not important for our cores.

If lateral transport of sediment initially deposited in shallower areas significantly affected paleoflux estimates, we would expect a correlation between the two. Fig. 7 shows no obvious correlation between the two because $F_{vertical}$ is virtually constant. Since this correlation is not observed, the redistributed sediment must come from an area of similar depth.

Consequently, we assume that the focusing factor represents more a measure of additional sediment deposited as well as additional $^{230}Th^{\circ}_{ex}$ deposited.

(3) Finally, there is another problem that leads to uncertainties in calculating the focusing factor. Namely, in order to use down-core variations of the focusing factor, one must assume that $^{230}Th_{ex}$ traces the redistribution of both biogenous and terrigenous components. This implies that ^{230}Th is distributed over all the particles without discrimination. In order to determine the degree to which particle composition influences the particle-reactive substances (like ^{230}Th, ^{231}Pa, ^{210}Pb and ^{10}Be), covariations between these substances activities and the major constituents (organic carbon, opal, carbonates and lithogenic fraction) were examined by different authors in the particulate matter collected by sediment traps.

No evidence was found for a relationship between radionuclide scavenging intensity and particle composition at the Nearshore site in the Southern Middle Atlantic Bight (for ^{230}Th, ^{231}Pa and ^{10}Be, Lao, 1991; Anderson, 1975) or in the Bay of Biscaye or off the Delmarva Peninsula (for ^{210}Pb, Biscaye and Anderson, 1994; Radakovitch and Heussner, 1999). These findings led the investigators to suggest that the composition of the particulate matter does not influence the initial partitioning of the chemical

species between solution and the solid phase in these regions. These situations are significantly different from those encountered in other areas, such as in the equatorial Pacific (for ^{230}Th, Luo and Ku, 1999), in the tropical northeast Atlantic (for ^{210}Pb, Legeleux et al., 1996), or in the eastern Equatorial Pacific (for ^{10}Be, Sharma et al., 1987), where the composition of particulate matter (aluminosilicates more particularly) influences the scavenging. Particle composition undoubtedly does influence scavenging under certain circumstances (Luo and Ku, 1999; Legeleux et al., 1996; Lao, 1991), and it appears that aluminosilicate may be the primary phase scavenging radionuclides in typical open ocean areas where the flux of total particulate matter is low (Biscaye and Anderson, 1994; Lao et al., 1993). However, it seems that in typical ocean-margin regions, where both terrigenous material flux and biological productivity are higher (Biscaye and Anderson, 1994; Lao, 1991; Anderson, 1975; Radakovitch and Heussner, 1999), the scavenging is regulated to a much stronger degree by the production, aggregation, and settling of particulate matter, i.e., the processes that contribute to the overall particle flux. In this latter case, ^{230}Th fluxes collected by sediment traps are well correlated with the total flux of organic matter, but not with the clay content of particles.

In our study, total particle fluxes are up to 14 times those occurring in typical open-ocean areas. Therefore, in the Indian sector of the Southern Ocean, where both terrigenous and biogenous material fluxes are high, it appears reasonable to compare this area to a typical ocean-margin region. The difference is that, in our case, the total particle fluxes are dominated by lateral fluxes of sediment; these conditions have also been observed by Biscaye and Anderson (1994) in the southern Middle Atlantic Bight, where no evidence was found for a relationship between radionuclide scavenging intensity and particle composition.

Having shown (1) that ^{230}Th is not preferentially scavenged by clays in regions where both terrigenous and biogenous material flux are high and (2) that the flux of ^{230}Th correlates well with the total flux of particulate matter, we assume that the focusing factor traces the redistribution of both biogenous and terrigenous components. Resolution of this assumption would require measurement of particle composition and ^{230}Th concentration in sediment traps in the Indian sector of the Southern Ocean.

References

Anderson, R.F., 1975. The marine geochemistry of thorium and protactinium. Ph.D. Thesis, Woods Hole Oceanographic Institution, Woods Hole, 287pp.

Anderson, R.F., 1982. Concentration, vertical flux, and remineralization of particulate uranium in seawater. Geochimica et Cosmochimica Acta 46, 1293–1299.

Anderson, R.F., Bacon, M.P., Brewer, P.G., 1983. Removal of ^{230}Th and ^{231}Pa from the open ocean. Earth and Planetary Science Letters 62, 7–23.

Anderson, R.F., Kumar, N., Froelich, P.N., Dittrich-Hannen, B., Sutter, M., 1998. Late-Quaternary changes in productivity of the Southern Ocean. Journal of Marine Systems 17, 497–514.

Anderson, R.F., Lao, Y., Broecker, W.S., Trumbore, S.E., Hofmann, H.J., Wolfli, W., 1990. Boundary scavenging in the Pacific Ocean: a comparison of ^{10}Be and ^{231}Pa. Earth and Planetary Science Letters 96, 287–304.

Bacon, M.P., 1984. Glacial to interglacial changes in carbonate and clay sedimentation in the Atlantic ocean estimated from ^{230}Th measurements. Isotope Geoscience 2, 97–111.

Bareille, G., 1991. Flux sédimentaires: paléoproductivité et paléocirculation de l'océan Austral au cours des 150,000 dernières années. Thèse, univ.de Bordeaux, p. 259.

Bareille, G., Grousset, F.E., Labracherie, M., Labeyrie, L.D., Petit, J.-R., 1994. Origin of detrital fluxes in the southeast Indian Ocean during the last climatic cycles. Paleoceanography 9 (6), 799–819.

Bareille, G., Labracherie, M., Bertrand, P., Labeyrie, L., Lavaux, G., Dignan, M., 1998. Glacial–interglacial changes in the accumulation rates of major biogenic components in Southern Indian Ocean sediments. Journal of Marine Systems 17, 527–539.

Bareille, G., Labracherie, M., Labeyrie, L., Pichon, J.J., Turon, J.L., 1991. Biogenic silica accumulation rate during the Holocene in the southeastern Indian Ocean. Marine Chemistry 35 (1–4), 537–551.

Barnola, J.M., Raynaud, D., Korotkevich, Y.S., Lorius, C., 1987. Vostok ice core provides 160,000-year record of atmospheric CO_2. Nature 329, 408–414.

Barron, J.A., Baldauf, J.G., Barrera, E., Caulet, J.-P., Huber, B.T., Keating, B.H., Lazarus, D., Sakai, H., Thierstein, H.R., Wei, W., 1991. Biochronologic and magnetochronologic sythesis of leg 119 sediments from the Kerguelen Plateau and Prydz Bay, Antarctica. Proceedings of the Ocean Drilling Program, Scientific Results, Vol. 119, College Station, TX, pp. 813–847.

Biscaye, P.E., Anderson, R.F., 1994. Fluxes of particulate matter on the slope of the southern Middle Atlantic Bight. Deep-Sea Research 41 (2/3), 459–509.

Boyle, E.A., 1988. Cadmium: chemical tracer of deepwater paleoceanography. Paleoceanography 3 (4), 471–489.

Charles, C.D., Fairbanks, R.G., 1990. Glacial to interglacial changes in the isotopic gradients of Southern Ocean surface water, geological history of the polar oceans: Arctic versus Antarctic In: Bleil, O., Thiede, J. (Eds.), Kluwer Academic Publishers, The Netherlands, pp. 519–538.

Charles, C.D., Froelich, P.N., Zibello, M.A., Mortlock, R.A., 1991. Biogenic opal in southern ocean sediments over the last 450,000 years: implications from the surface water chemistry and circulation. Paleoceanography 6, 697–728.

Cooke, D.W., Hays, J.D., 1982. Estimates of Antarctic ocean seasonal sea-ice cover during glacial intervals. In: Craddock, C. (Ed.), Antarctic Geoscience. University of Wisconsin Press, Madison, pp. 1017–1025.

Copin-Montegut, C., Copin-Montegut, G., 1978. The chemistry of particulate matter from the south Indian and Antarctic oceans. Deep-Sea Research 25, 911–931.

DeMaster, D.J., 1981. The supply and accumulation of silica in the marine environment. Geochimica et Cosmochimica Acta 45, 1715–1732.

Dosso, L., Bougault, H., Beuzart, P., Calvez, J.-Y., Joron, J.-L., 1988. The geochemical structure of the South-East Indian ridge. Earth and Planetary Science Letters 88, 47–59.

Duce, R.A., Tindale, N.W., 1991. The atmospheric input of trace species to the world ocean. Global Biochemical Cycles 5, 193–260.

Duplessy, J.C., Shackleton, N.J., Fairbanks, R.G., Labeyrie, L.D., Oppo, D., Kallel, N., 1988. Deep-water source variations during the last climatic and their impact on the global deep-water circulation. Paleoceanography 3, 343–360.

Ehrmann, W.U., Grobe, H., 1991. Cyclic sedimentation at sites 745 and 746. Proceedings of the ODP, Initial Reports, Vol. 119. pp. 225–235.

Eittreim, S., Bruchhausen, P.M., Ewing, M., 1972a. Vertical distribution of turbidity in the South Indian and South Australian Basins. Antarctica Research Series 19, 51–58.

Eittreim, S., Gordon, A.L., Ewing, M., Thorndike, E.M., Bruchhausen, P.M., 1972b. The nepheloid layer and observed bottom currents in the Indian-Pacific Antarctic Sea. In: Gordon, A. (Ed.), Studies in Physical Oceanography. Gordon & Breach, New York, pp. 19–35.

Elderfield, H., Hawkesworth, C.J., Greaves, M.J., 1981. Rare earth geochemistry of oceanic ferromaganese nodules and associated sediments. Geochimica et Cosmochimica Acta 45, 513–528.

Francois, R., Altabet, M.A., Yu, E.-F., Sigman, D.M., Frank, M., Bacon, M.P., Bohrmann, G., Bareille, G., Labeyrie, L.D., 1997. Contribution of southern ocean surface-water stratification to low atmospheric CO_2 concentrations during the last glacial period. Nature 389, 929–935.

Francois, R., Bacon, M.P., Altabet, M.A., Labeyrie, L.D., 1993. Glacial/interglacial changes in sediment rain rate in the SW Indian sector of Subantarctic waters as recorded by ^{230}Th, ^{231}Pa, U, and δ^{15}N. Paleoceanography 8 (5), 611–629.

Francois, R., Bacon, M.P., Suman, D.O., 1990. Thorium 230 profiling in deep-sea sediments: high-resolution records of flux and dissolution of carbonate in the equatorial Atlantic during the last 24,000 years. Paleoceanography 5 (5), 761–787.

Frank, M., 1996. Reconstitution of late Quaternary environmental conditions applying the natural radionuclides ^{230}Th, ^{10}Be, ^{231}Pa and ^{238}U: a study of deep-sea sediments from the eastern sector of the Antarctic Circumpolar Current System. In: Ph.D. Thesis. Alfred Wegener Institut, Bremerhaven, pp. 136.

Frank, M., Eisenhauer, A., Bonn, W.J., Walter, P., Grobe, H., Kubik, P.W., Dittrich-Hannen, B., Mangini, A., 1995. Sediment redistribution versus paleoproductivity change: Weddell Sea margin sediment stratigraphy and biogenic particle flux of the last 250,000 years deduced from $^{230}Th_{ex}$, ^{10}Be and biogenic barium profiles. Earth and Planetary Science Letters 136, 559–573.

Frank, M., Gersonde, R., Rutgers van der Loeff, M.M., Kuhn, G., Mangini, A., 1996. Late Quaternary sediment dating and quantification of lateral sediment redistribution applying $^{230}Th_{ex}$: a study from the eastern Atlantic sector of the Southern Ocean. Geol Rundsch 85, 554–566.

Grousset, F.E., Biscaye, P.E., Revel, M., Petit, J.-R., Pye, K., Joussaume, S., Jouzel, J., 1992. Antarctic (Dome C) ice core dust at 18 Kyr B.P.: isotopic constraints on origins. Earth and Planetary Science Letters 111, 175–182.

Houtz, R.E., Hayes, D.E., Markl, R.G., 1977. Kerguelen plateau bathymetry, sediment distribution and crustal structure. Marine Geology 25, 95–130.

Howard, W.R., Prell, W.L., 1992. Late Quaternary surface circulation of the southern Indian Ocean and its relationship to orbital variations. Paleoceanography 7, 79–117.

Jacobs, S.S., Amos, A.F., Bruchhausen, P.M., 1970. Ross Sea oceanography and Antarctic Bottom Water formation. Deep-Sea Research 17, 935–962.

Keigwin, L.D., Boyle, E.A., 1989. Late Quaternary paleochemistry of high-latitude surface waters. Paleogeography, Paleoclimatology, Paleoecology 73, 85–106.

Kennett, J.P., Watkins, N.D., 1975. Deep-sea erosion and manganese nodule development in the Southeast Indian Ocean. Science 188, 1011–1013.

Kennett, J.P., Watkins, N.D., 1976. Regional deep-sea dynamic processes recorded by late Cenozoic sediments of the southeastern Indian Ocean. Geological Society of America Bulletin 87, 321–339.

Klinck, J.M., Smith, D.A., 1993. Effect of wind changes during the last glacial maximum on the circulation in the Southern ocean. Paleoceanography 8, 427–433.

Knox, F., McElroy, M.B., 1984. Changes in atmospheric CO_2: influence of the marine biota at high latitudes. Journal of Geophysical Research 89, 4629–4637.

Kolla, V., Biscaye, P.E., 1976. Distribution and origin of quartz in the sediments of the Indian Ocean. Journal of Sedimentary Petrology 47, 642–649.

Kolla, V., Henderson, L., Biscaye, P.E., 1976a. Clay mineralogy and sedimentation in the western Indian ocean. Deep-Sea Research 23, 949–961.

Kolla, V., Henderson, L., Sullivan, L., Biscaye, P.E., 1978. Recent sedimentation in the southeast Indian ocean with special reference to the effects of Antarctic bottom water circulation. Marine Geology 27, 1–17.

Kolla, V., Sullivan, L., Streeter, S., Langseth, M., 1976b. Spreading of Antarctic bottom water and its effects on the floor of the Indian Ocean inferred from bottom-water potential temperature, turbidity, and sea-floor photography. Marine Geology 21, 171–189.

Ku, T.L., Knauss, K.G., Mathieu, G.G., 1977. Uranium in open ocean: concentration and isotope composition. Deep-Sea Research 19, 233–247.

Kumar, N., Anderson, R.F., Mortlock, R.A., Froelich, P.N., Kubik, P., Dittrich-hannen, B., Sutter, M., 1995. Increased biological productivity and export production in the glacial Southern Ocean. Nature 378, 675–680.

Labeyrie, L.D., Duplessy, J.C., 1985. Changes in the oceanic $^{13}C/^{12}C$ ratio during the last 140,000 years: high-latitude surface water records. Paleogeography, Paleoclimatology, Paleoecology 50, 217–240.

Labeyrie, L.D., Labracherie, M., Gorfti, N., Pichon, J.J., Vautravers, M., Arnold, M., Duplessy, J.C., Paterne, M., Michel, E., Duprat, J., Caralp, M., Turon, J.L., 1996. Hydrographic changes of the Southern Ocean (southeast Indian sector) over the last 230 Kyr. Paleoceanography 11 (1), 57–76.

Labeyrie, L.D., Pichon, J.J., Labracherie, M., Ippolito, P., Duprat, J., Duplessy, J.C., 1986. Melting history of Antarctica during the past 60,000 years. Nature 322, 701–706.

Lao, Y., 1991. Transport and burial rates of ^{10}Be and ^{231}Pa in the Pacific ocean. Ph.D. Thesis. Columbia University, p. 246

Lao, Y., Anderson, R.F., Broecker, W.S., Hofmann, H.J., Wolfi, W., 1993. Particulate fluxes of ^{230}Th, ^{231}Pa and ^{10}Be in the northeastern Pacific Ocean. Geochimica et Cosmochimica Acta 57, 205–217.

Legeleux, F., 1994. Relations entre particules marines et méssage sédimentaire: flux de matière dans la colonne d'eau et transformations à l'interface eau-sédiment dans l'océan Atlantique tropical du nordest. In: Ph.D. Thesis. Université Paris 6, Paris, p. 232.

Legeleux, F., Reyss, J.L., Etcheber, H., Khripounoff, A., 1996. Fluxes and balance of ^{210}Pb in the tropical northeast Atlantic. Deep-Sea Research 43 (8), 1321–1341.

Lemoine, F., 1998. Changements de l'hydrologie de surface (température et salinité) de l'ocean Austral en relation avec les variations de la circulation thermohaline au cours des deux derniers cycles climatiques, Ph.D. Thesis, 169, Université Paris 6, Paris. p. 169.

Luo, S., Ku, T.-L., 1999. Oceanic ^{231}Pa/^{230}Th ratio influenced by particle composition and remineralization. Earth and Planetary Science Letters 167, 183–195.

Manthe, S., Bareille, G., 2000. Variabilite des apports detritiques dans l'ocean austral au cours des derniers 30,000 ans. Oceanologica Acta, submitted for publication.

Martin, J.H., 1990. Glacial–Interglacial CO_2 change: the iron hypothesis. Paleoceanography 5 (1), 1–13.

McCave, 1986. Local and global aspects of the bottom nepheloid layers in the world ocean. Netherlands Journal of Sea Research 20 (2/3), 167–181.

Moore, W.S., Sackett, W.M., 1964. Uranium and thorium series inequilibrium in sea water. Journal of Geophysical Research 69, 5401–5405.

Mortlock, R.A., Charles, C.D., Froelich, P.N., Zibello, M.A., Saltzman, J., Hays, J.D., Burckle, L.H., 1991. Evidence for lower productivity in the Antarctic Ocean during the last glaciation. Nature 351, 220–223.

Mortlock, R.A., Froelich, P.N., 1989. A simple method for the rapid determination of biogenic opal in pelagic marine sediments. Deep-Sea Research 36, 1415–1426.

Nowlin, W.D., 1991. On water mass exchange between the Southern Ocean and the World Ocean: emphasis on the Atlantic sector. Marine Chemistry 35 (1–4), 1–7.

Orsi, A., Whitworth, T., Nowlin, W.D., 1995. On the meridional extent and fronts of the Antarctic Circumpolar Current. Deep-Sea Research 42, 641–673.

Palmer, M.R., 1995. Rare earth elements in foraminifera tests. Earth and Planetary Science Letters 73, 285–298.

Park, Y.H., Gambéroni, L., Charriaud, E., 1991. Frontal structure and transport of the Antarctic Circumpolar Current in the south Indian Ocean sector, 40–80°E. Marine Chemistry 35, 45–62.

Park, Y.H., Gambéroni, L., Charriaud, E., 1993. Frontal structure, water masses, and circulation in the Crozet Basin. Journal of Geophysical Research 98 (7), 12361–12385.

Park, Y.H., Saint-Guily, 1992. Sea level variability in the Crozet-Kerguelen-Amsterdam area from bottom pressure and Geosat altimetry. In: AGU, Washington, pp. 117–131.

Petit, J.R., Mounier, L., Jouzel, J., Korotkevitch, Y.S., Kotlyakov, V.I., Lorius, C., 1990. Paleoclimatological and chronological implications of the Vostok core dust record. Nature 343, 56–58.

Pudsey, C.J., 1992. Late Quaternary changes in Antarctic Bottom Water velocity inferred from sediment grain size in the northern Weddell Sea. Marine Geology 107, 9–33.

Radakovitch, O., Heussner, S., 1999. Fluxes and budget of ^{210}Pb on the continental margin of the Bay of Biscaye (Northeastern Atlantic). Deep-Sea Research II 46, 2175–2203.

Rintoul, S.R., 1998. On the origin and influence of Adélie Land Bottom Water. Ant. Res. Sevier, AGU 75, 151–171.

Salters, V.J.M., Storey, M., Sevigny, J.H., Whitechurch, H., 1992. Trace element and isotopic characteristics of Kerguelen-Heard plateau basalts. Proceedings of the Ocean Drilling Program 120, 55–62.

Sarmiento, J.L., Toggweiler, J.R., 1984. A new model for the role of the oceans in the determining atmospheric pCO_2. Nature 308, 621–624.

Sharma, P., Mahannah, R., Moore, W.S., Ku, T.L., Southon, J.R., 1987. Transport of ^{10}Be and ^{9}Be in the ocean. Earth and Planetary Science Letters 86, 69–76.

Sheraton, J.W., Black, L.P., Tindle, A.G., 1992. Petrogenesis of plutonic rocks in a Proterozoic granulite-facies terrane- the Bunger Hills, East Antarctica. Chemical Geology 97, 163–198.

Storey, M., Saunders, A.D., Tarney, J., Leat, P., Thirlwall, M.F., Thompson, R.N., Menzies, M.A., Marriner, G.F., 1988. Geochemical evidence for plume–mantle interactions beneath Kerguelen and Heard Islands, Indian Ocean. Nature 336, 371–374.

Suman, D.O., Bacon, M.P., 1989. Variations in Holocene sedimentation in the North American basin determined from ^{230}Th measurements. Deep-Sea Research 36 (6), 869–878.

Taylor, S.R., McLennan, S.M., 1985. The continental crust: its composition and evolution. Geoscience Texts, Oxford, 9. p. 312.

Walter, H.J., Rutgers van der Loeff, M.M., Hoeltzen, H., 1997. Enhanced scavenging of ^{231}Pa relative to ^{230}Th in the South Atlantic south of the Polar Front: implications for the use of the $^{231}Th/^{230}Th$ ratio as a paleoproductivity proxy. Earth and Planetary Science Letters 148, 85–100.

Weis, D., Frey, F.A., Giret, A., Gantagrel, J.-M., 1998. Geochemical characteristics of the youngest volcano (Mount Ross) in the Kerguelen Archipelago: Inferences for magma flux, lithosphere assimilation and composition of the Kerguelen plume. Journal of Petrology 39 (5), 973–994.